SPECIAL U.S. CLIVAR Hurricanes COLLECTION

Influence of Model Biases on Projected Future Changes in Tropical Cyclone Frequency of Occurrence*

HIROYUKI MURAKAMI

Department of Meteorology and International Pacific Research Center, University of Hawai'i at Mānoa, Honolulu, Hawaii, and Meteorological Research Institute, Tsukuba, Ibaraki, Japan

PANG-CHI HSU

Collaborative Innovation Center on Forecast and Evaluation of Meteorological Disasters, and College of Atmospheric Science, Nanjing University of Information Science & Technology, Nanjing, China, and Department of Meteorology and International Pacific Research Center, University of Hawai'i at Mānoa, Honolulu, Hawaii

OSAMU ARAKAWA

Meteorological Research Institute, and Faculty of Life and Environmental Sciences, University of Tsukuba, Tsukuba, Ibaraki, Japan

TIM LI

Department of Meteorology and International Pacific Research Center, University of Hawai'i at Mānoa, Honolulu, Hawaii

(Manuscript received 22 July 2013, in final form 25 November 2013)

ABSTRACT

The influence of model biases on projected future changes in the frequency of occurrence of tropical cyclones (FOCs) was investigated using a new empirical statistical method. Assessments were made of present-day (1979–2003) simulations and future (2075–99) projections, using atmospheric general circulation models under the Intergovernmental Panel on Climate Change (IPCC) A1B scenario and phase 5 of the Coupled Model Intercomparison Project (CMIP5) models under the representative concentration pathway (RCP) 4.5 and 8.5 scenarios. The models project significant decreases in global-total FOCs by approximately 6%–40%; however, model biases introduce an uncertainty of approximately 10% in the total future changes. The influence of biases depends on the model physics rather than model resolutions and emission scenarios. In general, the biases result in overestimates of projected future changes in basin-total FOCs in the north Indian Ocean (by +18%) and South Atlantic Ocean (+143%) and underestimates in the western North Pacific Ocean (−27%), eastern North Pacific Ocean (−29%), and North Atlantic Ocean (−53%). The calibration of model performance using the smaller bias influence appears crucial to deriving meaningful signals in future FOC projections. To obtain more reliable projections, ensemble averages were calculated using the models less influence by model biases. Results indicate marked decreases in projected FOCs in the basins of the Southern Hemisphere, Bay of Bengal, western North Pacific Ocean, eastern North Pacific, and Caribbean Sea and increases in the Arabian Sea and the subtropical central Pacific Ocean.

Denotes Open Access content.

* School of Ocean and Earth Science and Technology Publication Number 9046 and International Pacific Research Center Publication Number 1027.

Corresponding author address: Hiroyuki Murakami, International Pacific Research Center, 1680 East-West Road, University of Hawai'i at Mānoa, Honolulu, HI 96822.
E-mail: hir.murakami@gmail.com

DOI: 10.1175/JCLI-D-13-00436.1

1. Introduction

The effects of anthropogenic warming on tropical cyclone (TC) activity are critical for estimating the future costs of climate-related socioeconomic impacts. Recently, many studies have attempted to address future changes in TC activity using high-resolution atmospheric general circulation models (AGCMs) (e.g., Zhao et al. 2009; Bender et al. 2010; Murakami et al. 2012b; Knutson et al. 2013), atmosphere–ocean coupled general circulation models (CGCMs) (e.g., Yokoi et al. 2012; Mori et al. 2013), and statistical–dynamical models (e.g., Emanuel et al. 2008; Emanuel 2013). Most studies tend to show projected decreases in the TC genesis frequency globally (Knutson et al. 2010); however, projected changes in TC genesis frequencies are highly variable at interocean basin scales (e.g., Emanuel et al. 2008; Zhao et al. 2009; Knutson et al. 2010; Murakami et al. 2012a,b; Zhao and Held 2012). Models show substantial inconsistencies in projected regional changes in the frequency of occurrence of TCs (FOC), which is defined as the total count of TC positions for each analyzed grid cell (i.e., $10° \times 10°$) in a 6-h interval for all TCs during their lifetime. For example, Murakami et al. (2011), Yokoi and Takayabu (2009), and Yokoi et al. (2012) showed a projected eastward shift in the location of peak FOCs in the western North Pacific, whereas Murakami et al. (2012b) and Li et al. (2010) reported an overall decrease in FOCs in the basin. Murakami and Wang (2010) and Colbert et al. (2013) showed a projected eastward shift in the peak FOC in the North Atlantic, whereas Knutson et al. (2013) did not report such a shift in their projections.

Knutson et al. (2010), based on intermodel comparisons of fractional changes in TC activity, reported a wide range of genesis frequency changes at regional scales. To adequately estimate the range of projections associated with model variations, equal-weighted multimodel ensemble averages (EQW) would be a useful strategy. However, a number of questions remain regarding the multimodel ensemble approach. Is it appropriate to include models with marked biases in their control simulations as ensemble members? To what extent do biases in present-day simulations influence projected future changes in FOCs? Is it reasonable to assume that model biases do not substantially influence estimates of future changes, based on the assumption that subtracting simulated present-day means from projected future means offsets model biases? Figure 1 provides examples showing that the last assumption may not be applicable to projected future changes in FOCs; the figure compares projected future changes in FOCs (contours) with model biases in present-day simulations relative to observed FOCs (shadings), using two different models. For the bias (future change), as will be discussed in detail later in section 2, FOCs of the 25-yr present-day (future) experiment are subtracted from those of observed (present-day experiment) without any normalizations. The top panel shows a positive correlation in the Northern Hemisphere between the projected future changes and present-day model biases in FOCs, indicating that, if the model underestimates (overestimates) FOCs in the present-day simulation in a specific ocean basin, then it also tends to predict decreases (increases) in FOCs in the respective basins in the future. In contrast, the bottom panel shows a negative correlation in most of the basins between projected future changes and model biases in FOCs, indicating that, if the model underestimates (overestimates) FOCs in the present-day simulation, then it tends to predict increases (decreases) in FOCs in the respective basins in the future. In the positive correlation cases, it is possible that model biases in the present-day simulation are retained or amplified in the future projections. In the negative correlation cases, projected shifts in location of peak FOCs may be exaggerated because of the underlying model biases in FOCs in the present-day simulation. These marked correlations may indicate that present-day model biases could thus be inherited to the projections of future changes in FOCs.

To estimate the extent to which model biases in present-day simulations are inherited by projections of future changes in FOCs, we applied a new empirical statistical analysis that decomposes projected future changes into two components: 1) future changes related to model biases in the present-day simulation and 2) signals of future change representing results of a perfect model (i.e., biases are absent). We used simulation/projection results by 10 AGCMs developed by the Meteorological Research Institute (MRI) and 11 CGCMs from phase 5 of the Coupled Model Intercomparison Project (CMIP5) (Taylor et al. 2012; Camargo 2013; Tory et al. 2013) as case studies.

Our ultimate goal is to generate ensemble means using models that reduce the inheritance of biases to increase the reliability of information on projections of future changes in FOCs. On the other hand, the multimodel ensemble approach has been widely discussed in the literature for comprehensive forecast and projection frameworks such as short-range weather forecasting (Raftery et al. 2005; Casanova and Ahrens 2009), seasonal forecasting (Tippet et al. 2005; Casanova and Ahrens 2009), decadal prediction (Tippet 2006), and future climate projection (Perkins and Pitman 2009; Santer et al. 2009; Räisänen et al. 2010; Chen et al. 2011). A number of ensemble techniques such as skill-based weighing (Giorgi and Mearns 2003; Schmittner et al. 2005; Perkins and Pitman 2009; Santer et al. 2009), weighing based on intermodel similarity (Whetton et al. 2007; Räisänen et al. 2010), weighing using a signal-to-noise empirical orthogonal function (Tippet 2006), the statistical–dynamical method (Tippet et al. 2005), and Bayesian methods (Raftery et al.

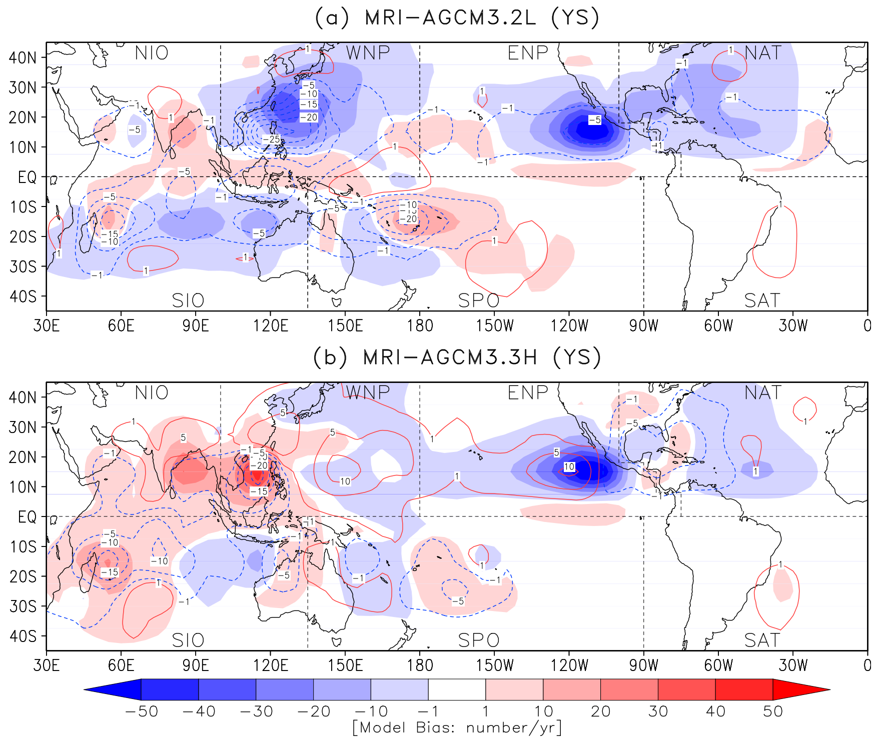

FIG. 1. Projected future changes in FOC (contours; TCs per year) superposed on model bias (shading; TCs per year), based on results of two models: (a) results of MRI-AGCM3.2L (YS) show a positive correlation case in the Northern Hemisphere between projected future changes and model biases and (b) results of MRI-AGCM3.3H (YS) show a negative correlation in most of the basins between projected future changes and model biases. The FOC is defined as a total count of TC positions in each analyzed 10° × 10° grid cell within the global domain in 6-h intervals. The abbreviations for the basins are given in the text.

2005; Casanova and Ahrens 2009) have also been proposed. In the context of the literature, the proposed methodology in this study is not novel because it is simply a skill-based weighing approach applied to climate projections. However, the application to tropical cyclone projections may be new because most of the literature focuses on temperature or precipitation fields.

The remainder of this paper is organized as follows: Section 2 describes the models, experimental design, and methods of analysis. Section 3 assesses the performance of present-day simulations and of projected future changes in FOCs and TC genesis frequencies. Next, the relationships between model biases and projected future changes in FOCs are examined and the ensemble mean approach is discussed. Finally, section 4 provides a summary of the results.

2. Methods

a. Models and simulation settings

Table 1 lists the models used in this study. We used 10 MRI-AGCMs representing different versions (versions 3.1, 3.2, and 3.3), different resolutions (20-, 60-, 120-, and 200-km mesh), and different cumulus convection schemes of the model. Version 3.1 of the MRI-AGCM, which is based on a global model developed by the Japan Meteorological Agency (JMA) and MRI (Mizuta et al. 2006), was developed to address potential future changes in TCs (Oouchi et al. 2006; Sugi et al. 2009; Murakami and Sugi 2010; Murakami and Wang 2010; Murakami et al. 2011). Version 3.2 was developed from version 3.1, with some modifications of the physical process components (Mizuta et al. 2012). Of particular relevance to this version is the use of a new cumulus convection scheme by Yoshimura (Yukimoto et al. 2011), which substantially improves the simulation of tropical precipitation and TC climatology (Mizuta et al. 2012; Murakami et al. 2012b). In version 3.3, which is very similar to version 3.2, several parameters in specific physical schemes were tuned to the MRI Earth System Model, version 1 (MRI-ESM1) (Yukimoto et al. 2011). To increase the sample sizes for the analyses, we also used results of 11 high-resolution CMIP5 models (with meshes finer than 200 km), which provide 6-hourly outputs for the TC-detection method that is described in section 2c.

TABLE 1. List of models used in this study. From left to right: model identifier (ID), model acronym, expanded model name, horizontal resolution, model-dependent criteria for TC detection (relative vorticity at 850 hPa and temperature anomaly), and model performance score in the present-day simulation of frequency of occurrence of tropical cyclones in terms of the root-mean-square error and the Taylor skill score II.

ID	Model name	Expanded model name	Horizontal resolution [lat × lon (km^2)]	TC detection criteria: ζ_{850} (m s^{-1})	TC detection criteria: t_a (°C)	Performance scores: RMSE	Performance scores: S_2
			MRI-AGCM versions				
A1	MRI-AGCM3.1S (AS)	MRI AGCM, version 3.1, super high resolution with Arakawa–Shubert scheme[a]	0.1875° × 0.1875° (20 × 20)	3.128×10^{-4}	1.0	6.59	0.68
A2	MRI-AGCM3.1H (AS)	MRI AGCM, version 3.1, high resolution with Arakawa–Shubert scheme	0.5625° × 0.5625° (60 × 60)	1.143×10^{-4}	1.0	7.45	0.55
A3	MRI-AGCM3.1M (AS)	MRI AGCM, version 3.1, medium resolution with Arakawa–Shubert scheme	1.1250° × 1.1250° (120 × 120)	8.330×10^{-5}	1.0	6.41	0.64
A4	MRI-AGCM3.1L (AS)	MRI AGCM, version 3.1, low resolution with Arakawa–Shubert scheme	1.8750° × 1.8750° (200 × 200)	7.680×10^{-5}	1.0	8.66	0.34
B1	MRI-AGCM3.2S (YS)	MRI AGCM, version 3.2, super high resolution with Yoshimura scheme[b]	0.1875° × 0.1875° (20 × 20)	3.540×10^{-4}	1.0	4.73	0.80
B2	MRI-AGCM3.2H (YS)	MRI AGCM, version 3.2, high resolution with Yoshimura scheme	0.5625° × 0.5625° (60 × 60)	1.000×10^{-4}	1.0	5.46	0.73
B4	MRI-AGCM3.2L (YS)	MRI AGCM, version 3.2, low resolution with Yoshimura scheme	1.8750° × 1.8750° (200 × 200)	5.360×10^{-5}	0.8	6.92	0.56
C2	MRI-AGCM3.2H (KF)	MRI AGM, version 3.2, high resolution with Kain–Fritsch scheme[c]	0.5625° × 0.5625° (60 × 60)	3.100×10^{-4}	1.0	4.30	0.83
D2	MRI-AGCM3.2H (AS)	MRI AGCM, version 3.2, high resolution with Arakawa–Shubert scheme	0.5625° × 0.5625° (60 × 60)	5.250×10^{-5}	0.5	8.40	0.53
E2	MRI-AGCM3.3H (YS)	MRI AGCM, version 3.3, high resolution with Yoshimura scheme	0.5625° × 0.5625° (60 × 60)	3.700×10^{-4}	1.0	6.55	0.69
			CMIP5 models				
1	CCSM4	Community Climate System Model, version 4	1.2500° × 0.9375° (130 × 100)	8.000×10^{-5}	1.0	7.93	0.41
2	CMCC-CM	Centro Euro-Mediterraneo per I Cambiamenti Climatici Climate Model	0.7500° × 0.7500° (80 × 80)	1.575×10^{-4}	1.0	5.50	0.75
3	CNRM-CM5	Centre National de Recherches Météorologiques Coupled Global Climate Model, version 5	1.4062° × 1.4062° (150 × 150)	4.500×10^{-5}	0.9	7.32	0.45
4	CSIRO Mk3.6.0	Commonwealth Scientific and Industrial Research Organisation Mark, version 3.6.0	1.8750° × 1.8750° (200 × 200)	7.550×10^{-5}	1.0	8.32	0.58
5	HadGEM2-CC	Hadley Centre Global Environment Model, version 2–Carbon Cycle	1.8750° × 1.2500° (200 × 130)	4.000×10^{-5}	1.0	6.90	0.61
6	HadGEM2-ES	Hadley Centre Global Environment Model, version 2–Earth System	1.8750° × 1.2500° (200 × 130)	6.100×10^{-5}	1.0	6.83	0.64
7	MIROC5	Model for Interdisciplinary Research on Climate, version 5	1.4062° × 1.4062° (150 × 150)	8.000×10^{-5}	1.0	6.74	0.64

TABLE 1. (*Continued*)

ID	Model name	Expanded model name	Horizontal resolution [lat × lon (km^2)]	TC detection criteria ζ_{850} (m s^{-1})	t_a (°C)	Performance scores RMSE	S_2
8	MPI-ESM-LR	Max Planck Institute Earth System Model, low resolution	1.8750° × 1.8750° (200 × 200)	4.000×10^{-5}	0.9	6.52	0.61
9	MPI-ESM-MR	Max Planck Institute Earth System Model, medium resolution	1.8750° × 1.8750° (200 × 200)	4.000×10^{-5}	0.7	6.82	0.58
10	MRI-CGCM3	MRI Coupled Atmosphere–Ocean General Circulation Model, version 3	1.1250° × 1.1250° (120 × 120)	1.560×10^{-4}	1.0	7.76	0.56
11	BCC_CSM1.1	Beijing Climate Center, Climate System Model, version 1.1	1.1250° × 1.1250° (120 × 120)	1.675×10^{-4}	1.0	8.04	0.51

[a] See Arakawa and Schubert (1974) and Randall and Pan (1993) for details.
[b] See Yukimoto et al. (2011) for details.
[c] See Kain and Fritsch (1990) for details.

Each model employed a pair of simulations: a present-day simulation (1979–2003) and a global-warmed future projection (2075–99). The simulation settings using in the MRI-AGCMs were identical to those used in our previous studies (Murakami and Sugi 2010; Murakami and Wang 2010; Murakami et al. 2011). Using a "time slice" method (Bengtsson et al. 1996), the AGCMs were forced by prescribed sea surface temperatures (SSTs) and sea ice concentrations (SICs) as the lower boundary conditions. The present-day simulations were styled after the Atmospheric Model Intercomparison Project (AMIP) models, in which the lower boundary conditions are prescribed by observed monthly mean SSTs and SICs during 1979–2003, obtained from the first Hadley Centre Global Sea Ice and Sea Surface Temperature dataset (HadISST1) (Rayner et al. 2003). In the CMIP5 models, the present-day simulation is based on so-called historical runs (Taylor et al. 2012), which are forced by observed atmospheric compositional changes reflecting anthropogenic and natural sources and sinks and time-evolving land-cover conditions.

The target for the future projections was the last quarter of the twenty-first century (2075–99). For the MRI-AGCMs, predicted mean changes and future trends in SSTs were estimated from models included in the phase 3 of the Coupled Model Intercomparison Project (CMIP3) (Meehl et al. 2007) developed under the Special Report of Emission Scenarios A1B scenario (Solomon et al. 2007); the anomalies were superposed on detrended mean observed SSTs for the period 1979–2003 while the high-frequency component (interannual variability) remains as the present-day climate (Mizuta et al. 2008). For the CMIP5 models, projection results under the representative concentration pathway (RCP) 4.5 and 8.5 scenarios (Taylor et al. 2012) were used in this study. Among the several ensemble members in the CMIP5 present-day and future simulations, only one ensemble member for each model was used in the simulations in this study. We note that the mean CO_2 concentration during the present-day period (1979–2003) is about 355 ppm, whereas the anticipated CO_2 concentration during the future period (2075–99) is 673, 533, and 820 ppm for the A1B, RCP4.5, and RCP8.5 scenarios, respectively, which is 1.9, 1.5, and 2.3 times greater than the present-day period.

b. *Observational datasets*

The observed TC "best track" data, obtained from the website of Unisys Corporation (Unisys 2013), were used to evaluate the TC simulations in the present-day run and to compute model biases. The dataset, which consists of best-track data compiled by the National Hurricane Center (NHC) and the Joint Typhoon Warning Center (JTWC), contains historical TC information regarding the locations of the centers of cyclones, cyclone intensities (maximum 1-min surface wind speeds), and sea level pressures at 6-hourly intervals from 1851 to 2009. We only used TCs with tropical storm intensities or stronger (i.e., TCs possessing 1-min sustained surface winds of 35 kt or greater; 1 kt $\approx$ 0.514 m s^{-1}) during the period 1979–2003.

c. *Detection algorithm for tropical cyclones*

Model-generated TCs were detected directly from 6-hourly output using the following model-dependent globally uniform criteria reported in Murakami and Sugi (2010):

1) The magnitude of the maximum relative vorticity at 850 hPa (ζ_{850}) exceeds a model-dependent threshold (Table 1).
2) The temperature structure aloft has a marked warm core, such that the sum of the temperature deviations

at the 300-, 500-, and 700-hPa vertical levels exceeds a model-dependent threshold (t_a in Table 1). The temperature deviation for each level was computed by subtracting the maximum temperature from the mean temperature in a surrounding 10° × 10° grid box. Because two pressure levels (i.e., 300 and 700 hPa) are not available in the CMIP5 output, the 250-, 500-, and 850-hPa vertical levels were used in the CMIP5 models.

3) The maximum wind speed at the 850-hPa vertical level is greater than that at 300 hPa (250 hPa for the CMIP5 models), in order to exclude extratropical cyclones.
4) The genesis position, defined as the first position at which criteria 1–3 are satisfied, is over the ocean.
5) The duration exceeds 36 h. Termination during a single time step is allowed to prevent double TC counts arising from detection and termination during the time step.

The model-dependent criteria in 1 and 2 are optimized for a given model configuration to ensure that the present-day global annual mean TC number matches observed values (84 per year for the period 1979–2003). We note that it is possible that analyzed results throughout this study are dependent on the selected TC-detection algorithm. For example, a unified detection algorithm used for all models could result in different results for model biases for some models because of resolution differences. We also note that differences in TC-detection algorithms result in discrepancies in projected future changes in TC frequency, even in the sign of the projected future change (discussed later in summary). Further study is required to address the dependency of the detection method on the results.

The TC positions in each 10° × 10° grid box were counted within the global domain at 6-h intervals. The total count for each grid box is defined as the FOC. The first detected position is defined as the location of TC genesis, and the frequency of occurrence of TC genesis (FOG) is counted similarly to that of the FOC. The analyses considered total global (GL) results and results for seven ocean basins: north Indian Ocean (NIO); western North Pacific (WNP); eastern North Pacific (ENP); North Atlantic (NAT); south Indian Ocean (SIO); South Pacific Ocean (SPO); and South Atlantic (SAT) (see Fig. 1 for regional boundaries).

d. Empirical statistical model of FOCs

A new empirical statistical analysis of FOCs can reveal the quantitative contributions of two factors to projected future changes in FOCs, 1) model biases and 2) signals of future change, on the assumption that the model predicting future change is not biased in its simulation of present-day conditions. The analysis, which was originally developed by Yokoi and Takayabu (2013) and Murakami et al. (2013a,b), is applied in the present study, with the modifications noted below.

First, we consider the FOCs in each analyzed grid cell (10° × 10°) within the global domain (50°S–50°N, over all longitudes). The FOC at a local grid cell A is influenced by both TC genesis frequency and track properties at remote grid cells A_0 so that the observed climatological mean of the FOC in a grid cell A can be expressed as an integration of the TC properties over the remote grid cells as follows:

$$\overline{f_o}(A) = \iint_C \overline{g_o}(A_0)\overline{t_o}(A, A_0)\, dA_0, \tag{1}$$

where $f(A)$ is the FOC in grid cell A, $g(A_0)$ is the FOG in remote grid cell A_0; $t(A, A_0)$ is the probability that a TC generated in grid cell A_0 travels to grid cell A; and C is the global domain over which the integration is performed. The subscript o for f, g, and t indicates the observed value. An overbar indicates the climatological mean value.

The simulated present-day mean FOC, with an accounting of model biases, is computed as

$$\begin{aligned}\overline{f_p}(A) &= \overline{f_o}(A) + f_b'(A)\\ &= \iint_C [\overline{g_o}(A_0) + g_b'(A_0)][\overline{t_o}(A, A_0) + t_b'(A, A_0)]\, dA_0,\end{aligned} \tag{2}$$

where the subscripts p and b represent present-day means and model biases, respectively, and a prime symbol indicates an anomaly (in this case, a model bias). Likewise, the projected future mean FOC is computed as

$$\begin{aligned}\overline{f_f}(A) &= \overline{f_p}(A) + f_c'(A) = \overline{f_o}(A) + f_b'(A) + f_c'(A)\\ &= \iint_C [\overline{g_o}(A_0) + g_b'(A_0) + g_c'(A_0)][\overline{t_o}(A, A_0) + t_b'(A, A_0) + t_c'(A, A_0)]\, dA_0,\end{aligned} \tag{3}$$

where the subscripts f and c represent the projected future value and the future change, respectively. Subtracting Eq. (2) from Eq. (3) yields the projected future change in the FOC expressed as

$$df(A) = \underbrace{\underbrace{\iint_C \overline{g_o}(A_0) t'_c(A, A_0)\, dA_0}_{T_s} + \underbrace{\iint_C g'_c(A_0) \overline{t_o}(A, A_0)\, dA_0}_{G_s} + \underbrace{\iint_C g'_c(A_0) t'_c(A, A_0)\, dA_0}_{N_s}}_{df_s}$$

$$+ \underbrace{\underbrace{\iint_C g'_b(A_0) t'_c(A, A_0)\, dA_0}_{G_b} + \underbrace{\iint_C g'_c(A_0) t'_b(A, A_0)\, dA_0}_{T_b}}_{df_b} . \qquad (4)$$

Equation (4) reveals the contribution of five factors integrated over the entire domain to the projected future change in the FOC in a given grid cell. The first three terms in Eq. (4) ($\equiv df_s$) are signals of future changes based on the assumption that the model simulates observed FOCs perfectly (i.e., without biases). The three terms consist of the TC track effect T_s, TC genesis effect G_s, and a combined nonlinear effect N_s. In contrast, the last two terms in Eq. (4) ($\equiv df_b$) are signals of future changes related to interactions between the model biases and the future changes. The two terms consist of future changes related to biased estimates of the FOG G_b and biased estimates of the TC track property T_b.

Our analysis indicates domain-wide effects of TC activity on local FOCs. For example, the magnitude of G_s implies that varying FOGs generate local FOC changes, while TC track properties (e.g., moving directions and speeds) are kept as observations over the global domain. If the magnitude of this term is greater than that of other terms for the grid cell A, then projected changes in FOG somewhere in the domain must have a large impact on FOC changes in grid cell A. Note that, if the model biases are zero, then future change in FOCs can be computed from only the first three terms; thus, the ratio of the summed magnitudes of the bias terms to the magnitudes of the total future change in FOCs (RBTC; i.e., df_b/df) can be regarded as the degree to which model biases are inherited in projected future changes in FOCs, which can be represented as

$$\mathrm{RBTC} \equiv \begin{cases} df_b/df & (df \neq 0) \\ df_b/f_p & (df = 0 \wedge f_p \neq 0) \\ \text{null} & (df = 0 \wedge f_p = 0) \end{cases} , \qquad (5)$$

where f_p is the mean value of the FOC in the present-day simulation.

The RBTC is a normalized value with a positive or negative sign. The schematic in Fig. 2 shows the implications of the magnitudes and signs of the RBTC. In the ideal case, the value of the RBTC is zero (Fig. 2a), as the model contains no biases (i.e., the model is perfect); in this case, projected future changes are not influenced by model biases. Smaller absolute magnitudes of the RBTC imply less influence of model biases on projected future changes. If the value of the RBTC is greater than 1, this indicates that projections of future changes are unreliable, as the future changes associated with the model biases are greater than the total projected future change. A positive value of the RBTC (Fig. 2b) indicates that the model overestimates future changes on account of the bias terms (i.e., $df > df_s$), whereas a negative value of the RBTC (Fig. 2c) indicates that the model underestimates projected changes on account of the bias terms (i.e., $df < df_s$). If the projected future change is zero (Fig. 2d), the present-day mean value f_p is used to normalize for the RBTC. If df and f_p are both zero, RBTC is set to a null value in this study.

Note that model biases in future simulations that we are unable to be address are not considered. The biases in the future simulations may be included in the signal of the future change term [df_s in Eq. (4)] as well as the bias term. If the model biases in the future are identical to those in the present day, the bias term in Eq. (4) df_b would be offset by a part of the future change term df_s; therefore, model biases do not always contribute to the total change in the FOCs. However, because observations in the future are not available, it is beyond the scope of this study to estimate the biases associated with future simulations. In this study, we only address the relationships between the model biases in the present-day simulations and the total projected future changes.

As discussed in section 1, we generate ensemble means using models that reduce the inheritance of biases (i.e., models with small RBTC) to increase the reliability of future projections. Although there are a number of possible methods to average the models, we selected models with RBTC $\leq$ 0.5 for each basin in this study as a preliminary step. The threshold value of 0.5 is arbitrary and subjective; however, our preliminary study suggests that ensemble means are not sensitive to the threshold value when it ranges from 0.25 to 1.0. The proposed ensemble

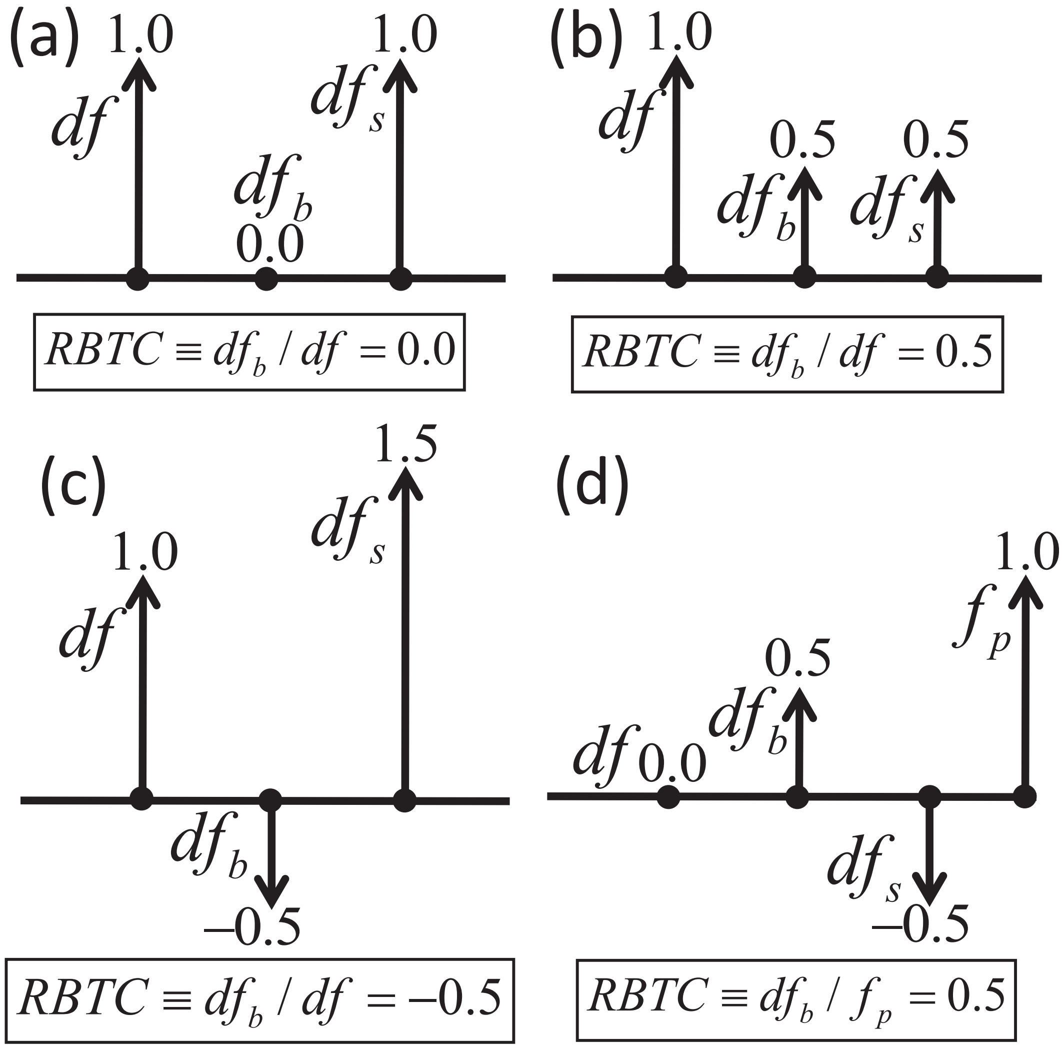

FIG. 2. Schematic diagram explaining the ratio of the sum of the bias terms df_b to the total projected change df (referred to as the RBTC). (a) In this case, $df_b = 0$, $df = df_s$, and RBTC = 0. (b) When df_b and df_s are both positive (i.e., RBTC > 0), the projected future changes are overestimated (i.e., $df > df_s$). (c) When df_b is negative (RBTC < 0), projected future changes are underestimated (i.e., $df < df_s$). (d) A special case, in which df_b and df_s are of the same magnitude but with opposite signs, such that the projected future changes equal zero. In this case, the present-day mean value f_p is used to normalize for the RBTC.

approach using RBTC threshold eliminates some ''bad'' climate models that show larger influence of biases, which differs from the downweighting approach (e.g., Chen et al. 2011) where all models have a nonzero weight even if the model performance is bad. Therefore, it is possible that the ensemble mean in a specific basin could be determined by using single model if the rest of the models show larger RBTC. In section 3d, the ensemble means using models with RBTC $\leq$ 0.5 will be compared with those using EQW and models with the five highest S_2 scores. As will be shown later, one of the advantages using models with smaller RBTC for the ensemble mean is that we can get the ensemble mean with smaller RBTC than EQW and models with the five highest S_2 scores, leading to greater confidence in quantitative analyses on future changes.

3. Results

a. Present-day performance

A Taylor diagram (Taylor 2001) (Fig. 3) was used to evaluate model performance in terms of the global distribution of FOCs in the present-day simulation. Table 1 lists the root-mean-square error (RMSE) and the Taylor skill score II (S_2; Taylor 2001) for each model; S_2 is defined as

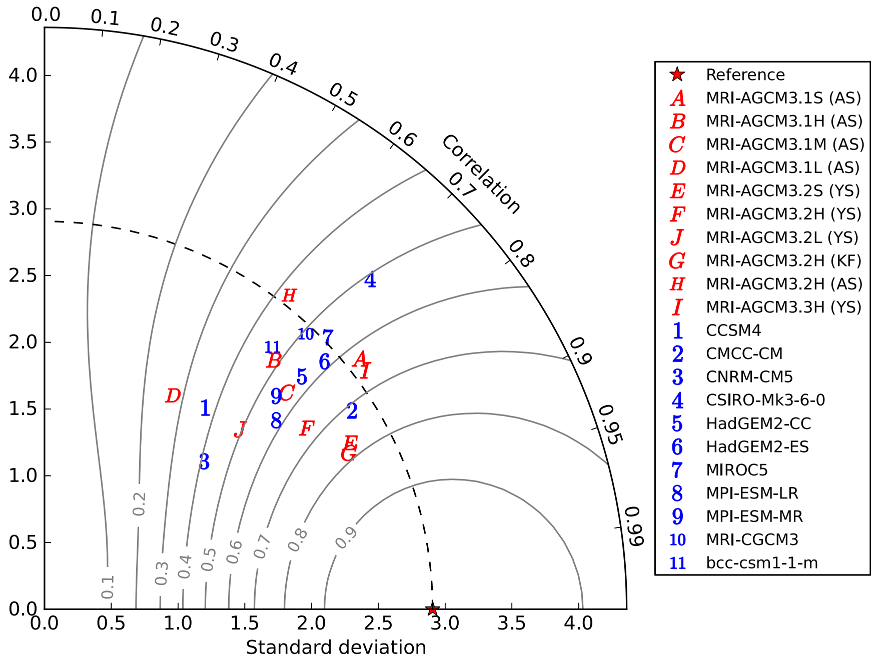

FIG. 3. Taylor diagram showing evaluations of the simulated global distribution of FOCs vs best-track data defined as reference. The different models are represented according to the inset legend. The dashed line represents results for the reference standard deviation. The solid contours represent values of S_2 as defined in Eq. (6). The star mark indicates reference used from the best-track data.

$$S_2 = \frac{4(1+R)^4}{(\hat{\sigma}_f + 1/\hat{\sigma}_f)^2(1+R_0)^4}, \qquad (6)$$

where R is the spatial correlation coefficient between simulated and observed FOC fields, R_0 is the maximum correlation attainable (1.0 for simplicity), and $\hat{\sigma}_f$ indicates modeled standard deviation in the global distribution of FOCs normalized by corresponding observed values. The parameter S_2, which represents the combined influence of the spatial variance and spatial correlation, ranges from 0.0 (no skill) to 1.0 (perfect skill level). Figure 3 reveals that the models with the highest skill level are the high-resolution MRI-AGCMs (models E and G) followed by a CMIP5 model of the CMCC-CM (model 2). When the MRI-AGCMs are compared, the finer-resolution models tend to show higher skill levels in terms of S_2, indicating that high-resolution models are generally desirable for accurate simulations of TC spatial distributions (Murakami and Sugi 2010; Walsh et al. 2013). However, this relationship is not clear in the CMIP5 models, except in the case of the finest-resolution model of the CMCC-CM (80-km mesh), which shows the highest skill level. The models also tend to show smaller standard deviations than observations, indicating that models underestimate spatial contrast in the FOC distribution.

b. *Projected future changes in the TC genesis frequency and FOC*

Tables 2 and 3 show projected future changes in the TC genesis frequency and the basin-total FOC, respectively, for each experiment and for each basin. Overall, projected future changes in FOCs correspond to those of TC genesis frequency, indicating that changes in the TC genesis frequency are a primary contributor to changes in the basin-total FOC. Most of the models show marked and statistically significant reductions in the TC genesis frequency and the FOC in the GL (by 15%–29% for A1B; by 6%–23% for RCP4.5; and by 13%–40% for RCP8.5), which is likely to be proportional to the anticipated mean CO_2 concentration in the future. However, a few CMIP5 models under RCP8.5 scenario show a marked projected increase in global TC number (i.e., models 1, 2, and 11) that is consistent with recent studies by Camargo (2013) and Emanuel (2013) but inconsistent with Tory et al. (2013). The substantial increases shown by these models are mostly attributed to increases in TC number in the NIO, WNP, and ENP. Further analyses are needed to explain the physical reasons for these increases; however, the above results may imply that the projected future change in global TC number is not always linear to the fractional increase in CO_2 concentration but are model dependent.

TABLE 2. Fractional changes in the annual mean frequency of tropical cyclone genesis (%) according to the different models (from top to bottom: MRI-AGCM A1B, CMIP5 RCP4.5, and CMIP5 RCP8.5). Statistically significant changes (by the bootstrap method) are highlighted according to the level of significance: 99%, 95%, and 90% (see footnotes). Model IDs are given in Table 1. The ensemble means shown are equal averages of the models (EQW), models with RBTC ≤ 0.5, and models with the five highest S_2 scores (S_2 Top5).

Model ID	GL	NIO	WNP	ENP	NAT	SIO	SPO	SAT
				MRI-AGCM A1B				
A1	−15.8[a]	−11.8	−26.8[a]	−14.5	+5.6	−4.8	−34.9[a]	−7.7
A2	−18.8[a]	+18.0	−11.7	−30.5[a]	+4.2	−8.9	−33.7[a]	−38.5
A3	−29.0[a]	−2.8	−26.0[b]	−24.7[a]	−14.2	−32.7[a]	−62.8[a]	+50.0
A4	−1.2	+22.1	−18.5[b]	+17.3[c]	+56.7[a]	−17.0[b]	−14.3[c]	+11.1
B1	−16.9[a]	−10.6	−19.0[b]	−4.4	−21.1[b]	−23.6[b]	−30.4[a]	+44.4
B2	−25.0[a]	−16.0	−29.5[a]	−12.9	−45.4[a]	−25.4[a]	−24.5[b]	−30.0
B4	−23.0[a]	−16.0	−22.5[a]	−25.3[b]	−36.5[b]	−30.8[a]	−19.5[b]	+200.0[b]
C2	−17.5[a]	−30.5[a]	−24.2[a]	−6.2	−28.8[b]	−23.8[a]	−4.5	+116.7[c]
D2	−16.8[a]	+0.9	−13.3	−17.8	−12.5	−24.2[a]	−31.8[a]	+100.0
E2	−0.4	+9.2	+7.9	+65.3[a]	−25.0[c]	−26.3[a]	−8.2	+91.7[c]
EQW	−16.4[a]	−4.1	−17.1[a]	−12.0[c]	−13.9	−21.6[a]	−25.0[a]	+39.7[b]
RBTC ≤ 0.5	−17.6[a]	−7.3	−17.3[a]	−15.6[b]	−14.3	−22.8[a]	−29.9[a]	+58.3
S_2 Top5	−15.1[a]	−10.0	−14.1[b]	−18.6[a]	−13.9	−25.9[a]	−25.1[a]	+59.7[a]
				CMIP5 RCP4.5				
1	−7.0[b]	−4.4	+8.6	−6.6	−26.9	−14.5[b]	−11.6	−73.5[a]
2	−5.0[c]	+2.6	−0.9	+27.6[a]	−13.4	−20.9[a]	−18.7[a]	−45.2[a]
3	−10.1[a]	−24.4[b]	−11.0[c]	−0.6	−20.6[c]	−11.9[b]	−8.4[c]	−5.6
4	−15.8[a]	+20.5[c]	+3.6	−26.0[b]	−46.2[b]	−36.1[a]	−19.2[b]	0.0
5	−16.0[a]	+21.1	−2.0	+15.5	−16.3	−29.7[a]	−30.8[a]	−42.1
6	−15.6[a]	−6.1	−14.6[a]	+26.8[b]	−19.2	−27.1[a]	−26.1[a]	+50.0
7	−23.3[a]	−3.9	−33.2[a]	−26.8[a]	−13.9	−21.6[a]	−30.2[a]	+4.0
8	−6.6[b]	−1.7	−5.4	+6.8	−28.2[b]	−9.3	−7.7	−13.2
9	−3.4	−14.1	−2.3	+31.4[a]	−30.2[b]	−14.1[b]	+9.9	−26.2[b]
10	−2.0	+10.3	+7.1	+12.9	+14.3	−15.8[a]	−3.2	−29.6
11	−0.5	−11.3	+1.7	+0.6	+14.7	−6.0	+6.7	−47.1[c]
EQW	−9.6[a]	−3.1	−3.4	+5.0[b]	−20.6[a]	−19.8[a]	−12.8[a]	−22.2[a]
RBTC ≤ 0.5	−14.8[a]	−7.0	−5.0[c]	+4.3	−20.6[c]	−19.8[a]	−24.0[a]	+50.0
S_2 Top5	−13.3[a]	−3.1	−0.7	+7.5[b]	−21.9[a]	−18.0[a]	−13.5[a]	−27.6[a]
				CMIP5 RCP8.5				
1	+7.8[b]	−1.8	+12.3	+38.6[a]	−46.2[a]	−0.9	−13.8	−41.2[c]
2	+33.5[a]	+97.4[a]	+29.7[a]	+101.5[a]	+1.8	−15.3[a]	+17.1[a]	−18.3
3	−19.7[a]	−28.6[b]	−26.0[a]	−14.2[c]	−14.3	−22.4[a]	−13.8[a]	−13.6
4	−21.6[a]	+1.7	−5.0	−1.1	−55.8[b]	−47.4[a]	−11.7	−71.4[c]
5	−35.5[a]	+1.8	−19.4[a]	−9.1	−40.7[a]	−51.5[a]	−46.8[a]	−42.1
6	−40.4[a]	−36.4[b]	−26.2[a]	−14.8[c]	−23.1	−57.2[a]	−49.6[a]	−25.0
7	−32.3[a]	+0.4	−47.1[a]	−34.9[a]	−12.7	−37.3[a]	−34.9[a]	−32.0
8	−14.9[a]	−27.5[a]	−12.1[b]	+21.5[b]	−54.6[a]	−26.5[a]	−15.8[c]	−18.2
9	−13.2[a]	−36.5[a]	−15.8[a]	+30.8[a]	−48.6[a]	−23.6[a]	+2.2	−21.5
10	−2.4	+28.7[b]	+2.0	+23.3[b]	+32.1	−24.1[a]	+5.7	−33.3
11	+5.6[b]	+12.6	+11.3[c]	+4.5	−5.9	−6.9	+12.4[b]	−23.5
EQW	−12.1[a]	+2.8	−7.3[a]	+17.0[a]	−28.9[a]	−30.8[a]	−14.4[a]	−22.2[a]
RBTC ≤ 0.5	−15.4[a]	−15.0[a]	−6.7[a]	+12.3[a]	−40.7[a]	−33.1[a]	−39.4[a]	−71.4[c]
S_2 Top5	−17.9[a]	+15.7[a]	−3.2	+16.0[a]	−28.4[a]	−25.7[a]	−24.4[a]	−20.4[a]

[a] Statistically significant at 99% level.
[b] Statistically significant at 95% level.
[c] Statistically significant at 90% level.

The projected reductions are also substantial and robust in the Southern Hemispheric ocean basins (SIO and SPO), a result that is consistent with the findings of previous studies (e.g., Knutson et al. 2010; Murakami et al. 2012b). Most of the MRI-AGCMs under the A1B scenario project marked reductions in TC genesis frequency and FOCs in the WNP and ENP; however, the fractional ratios vary substantially among the models (by 5%–30%). Projected future changes in both TC genesis frequency and FOCs by the CMIP5 models under RCP4.5 and RCP8.5 scenarios are highly variable in the WNP and ENP. Moreover, even the

TABLE 3. As in Table 2, but for projected future changes in basin-total FOCs. Boldface and italic fonts indicate the magnitude of the ratio of bias term to total future change (i.e., |RBTC| ≤ 0.25 and ≤0.5, respectively).

Model ID	GL	NIO	WNP	ENP	NAT	SIO	SPO	SAT
				MRI-AGCM A1B				
A1	**−8.9**[c]	**−7.6**	**−20.8**[c]	+0.1	**+16.0**	**−2.4**	**−37.9**[a]	−9.6
A2	**−16.2**[a]	**+11.5**	−6.5	**−25.5**[a]	*+4.1*	*−12.2*	**−35.7**[a]	−41.6
A3	**−27.0**[a]	**+8.4**	**−23.1**[b]	**−18.2**[b]	*−1.6*	**−39.5**[a]	**−62.5**[a]	**+32.9**
A4	−1.3	**+28.3**[c]	−21.6[b]	*+30.9*[a]	*+67.8*[a]	**−26.6**[a]	−6.0	−2.1
B1	**−21.0**[a]	*−20.8*[c]	**−26.7**[a]	**+2.0**	**−17.3**	**−26.5**[b]	**−42.8**[a]	−8.7
B2	**−30.8**[a]	**−22.2**[b]	**−37.5**[a]	−5.0	−51.8[a]	**−30.7**[a]	**−32.1**[a]	−1.2
B4	*−30.4*[a]	**−18.4**	**−33.4**[a]	*−29.5*[b]	−42.0[b]	**−36.1**[a]	**−26.9**[a]	*+314.9*[b]
C2	**−16.4**[a]	**−32.1**[a]	**−28.3**[a]	**−3.3**	*−19.5*	**−17.8**[b]	−1.1	*+132.1*[c]
D2	*−11.5*[a]	+9.6	**−8.2**	*−16.3*	−20.2	*−15.5*[b]	**−28.3**[a]	**+135.7**
E2	**−3.0**	+0.3	**+9.6**	**+51.3**[a]	**−32.8**[b]	**−24.0**[a]	**−7.3**	*+181.9*[c]
EQW	**−16.4**[a]	**−5.4**	**−18.7**[a]	*−4.9*	**−12.8**	**−21.5**[a]	**−27.1**[a]	*+49.2*[b]
RBTC ≤ 0.5	**−17.0**[a]	**−7.9**	**−19.1**[a]	*−9.2*	**−12.3**	**−23.4**[a]	**−33.7**[a]	**+47.5**
S_2 Top5	**−15.6**[a]	**−9.1**	**−16.5**[b]	**−9.2**	**−11.5**	**−25.6**[a]	**−27.2**[a]	*+83.4*[a]
				CMIP5 RCP4.5				
1	−5.8	**+6.0**	+4.0	−5.4	−29.0	**−10.4**	**−16.1**	−80.4[a]
2	*−3.3*	+3.2	**+6.9**	**+24.3**[a]	−6.1	**−21.9**[a]	**−15.5**[a]	*−38.8*[b]
3	*−10.8*[a]	**−19.8**[c]	−16.6[b]	−5.2	**−11.7**	**−9.9**[b]	−5.8	−6.9
4	**−15.5**[a]	+1.8	*+10.8*[b]	**−36.5**[a]	−48.1[a]	**−42.0**[a]	−1.4	*+14.5*
5	**−21.4**[a]	+5.9	**−6.8**	+13.4	−8.5	**−36.1**[a]	**−33.1**[a]	−42.6
6	**−23.4**[a]	−3.1	**−17.0**[a]	+17.9[c]	−7.8	**−36.0**[a]	**−32.4**[a]	**+46.8**
7	**−29.0**[a]	*−7.0*	*−39.6*[a]	**−36.6**[a]	+1.5	**−27.4**[a]	**−34.4**[a]	+3.8
8	*−8.3*[a]	**−7.6**	*−9.5*	**+8.8**	−32.5[b]	**−12.0**[c]	*−4.8*	−8.8
9	**−10.0**[a]	*−19.9*[b]	**−12.5**[b]	**+33.6**[a]	−39.3[a]	**−13.8**[b]	−2.9	*−37.4*[a]
10	−2.9	**+20.4**	*+7.0*	+19.4[c]	+25.2	**−17.5**[a]	−3.5	−38.0
11	+0.3	**−3.0**	*+6.2*	−16.8	+33.4	**−6.3**	+3.0	−29.4
EQW	**−11.8**[a]	**−2.1**	**−3.9**	+0.5	*−18.1*[a]	**−23.4**[a]	**−14.1**[a]	−24.3[a]
RBTC ≤ 0.5	**−20.2**[a]	+0.8	**−6.2**[c]	−1.4	**−11.7**	**−23.4**[a]	**−26.2**[a]	**+46.8**
S_2 Top5	**−17.2**[a]	−3.4	+2.1	+0.4	−19.6[a]	**−19.6**[a]	**−17.7**[a]	−26.4[a]
				CMIP5 RCP8.5				
1	+8.7[c]	*+17.0*[c]	**+17.3**	*+38.3*[a]	*−49.0*[b]	−0.2	*−19.7*	−52.2[b]
2	**+22.8**[a]	*+75.3*[a]	**+26.1**[a]	**+96.9**[a]	+7.0	**−23.0**[a]	*+3.2*	−18.2
3	**−21.3**[a]	**−27.0**[b]	*−31.6*[a]	**−13.5**	−12.8	**−22.8**[a]	*−13.1*[b]	−12.6
4	**−20.6**[a]	−16.7	+4.5	−4.4	−63.8[a]	**−54.3**[a]	+16.8	**−56.4**
5	**−43.0**[a]	−6.6	**−23.3**[a]	**−21.2**[b]	**−39.2**[b]	**−62.4**[a]	**−48.8**[a]	−42.6
6	**−48.2**[a]	**−45.9**[a]	**−28.7**[a]	**−27.7**[a]	*−8.0*	**−66.7**[a]	**−54.6**[a]	−36.1
7	**−37.2**[a]	−1.6	**−51.1**[a]	**−38.3**[a]	+2.3	**−46.6**[a]	**−30.9**[b]	−55.4[b]
8	**−22.5**[a]	**−33.4**[a]	**−23.6**[a]	**+14.4**	*−62.5*[a]	**−27.7**[a]	**−22.8**[b]	−29.0[c]
9	**−21.9**[a]	**−40.1**[a]	**−27.3**[a]	*+27.4*[a]	−58.5[a]	**−26.3**[a]	*−12.8*[c]	−33.0[b]
10	*−9.9*[a]	**+31.2**[c]	+1.8	**+21.7**[c]	+39.8	**−31.2**[a]	−7.8	−36.6
11	**+9.0**[a]	**+17.8**	**+21.6**[a]	−15.2	+35.5	**−5.1**	+7.8	−9.8
EQW	**−15.7**[a]	+4.0	**−6.6**[b]	**+12.7**[a]	−28.4[a]	**−36.3**[a]	**−17.4**[a]	−27.7[a]
RBTC ≤ 0.5	**−19.2**[a]	**−12.7**[b]	**−7.5**[b]	**+9.2**[a]	**−39.2**[b]	**−39.4**[a]	**−42.0**[a]	**−56.4**
S_2 Top5	**−23.9**[a]	+10.6[b]	−1.0	**+11.3**[a]	−29.1[a]	**−29.1**[a]	**−28.8**[a]	−22.4[b]

[a] Statistically significant at 99% level.
[b] Statistically significant at 95% level.
[c] Statistically significant at 90% level.

signs of the future changes are inconsistent among the CMIP5 models. The results of both the MRI-AGCMs under A1B scenario and CMIP5 models under the RCP4.5 scenario tend not to show significant and robust changes in TC genesis frequency and FOCs in the NIO, NAT, and SAT relative to changes in other ocean basins.

c. *Relationships between model bias and projected future changes in FOCs*

As shown in Fig. 1, the spatial distribution of projected future changes in FOCs may, in certain circumstances, be approximately correlated with that of model biases. Figure 4 shows spatial correlation coefficients

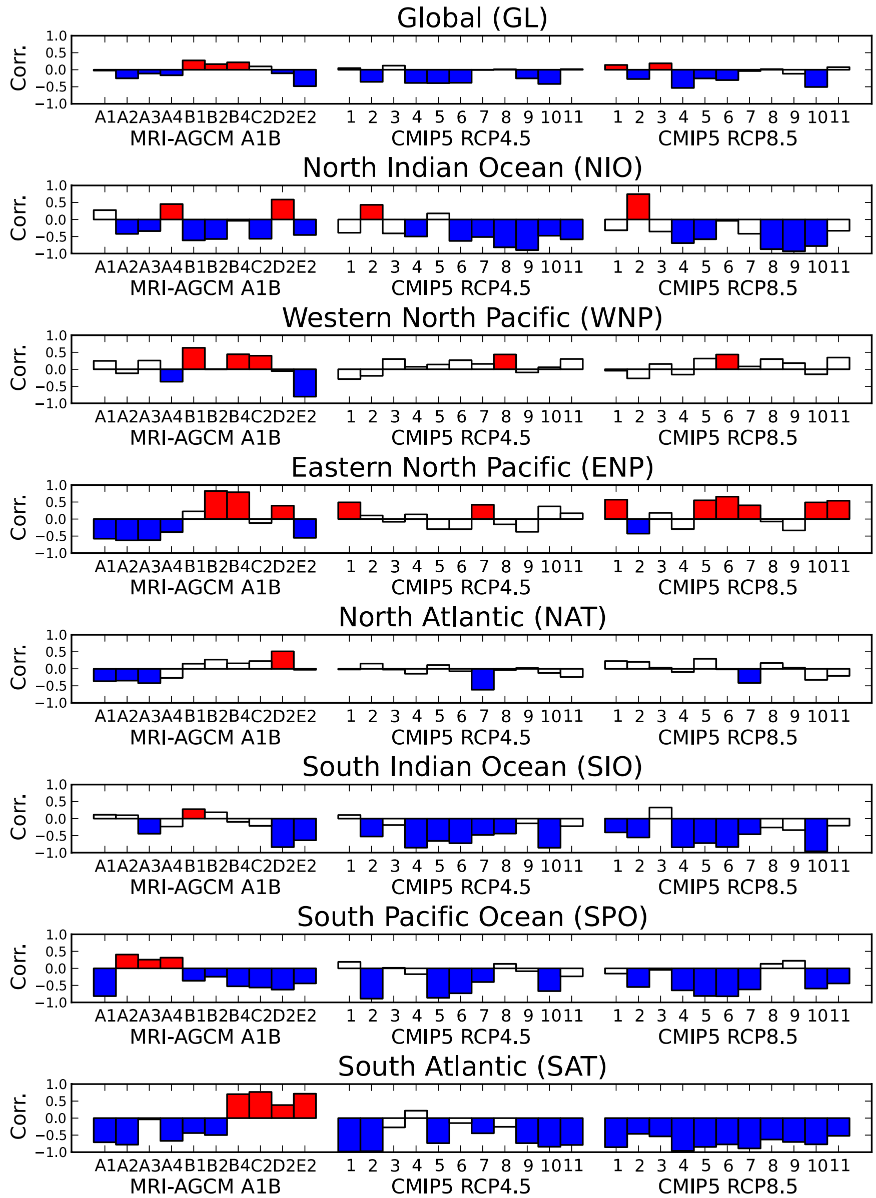

FIG. 4. Correlations between spatial distributions of model bias and projected future changes in FOCs in each basin (one chart per basin) and for each model (horizontal axes). Red (blue) bars indicate that the positive (negative) correlation coefficients are statistically significant at the 95% level (significance test for Pearson's product–moment correlation). Model IDs are given in Table 1.

between the model biases and projected future changes in FOCs for each model and for each ocean basin. Overall, the sign of the correlation depends on the model and ocean basin considered. When the MRI-AGCMs under the A1B scenario are compared with one another (i.e., left side of each panel in Fig. 4), the signs of the correlations vary depending on the model version and the cumulus convection scheme used, rather than on model resolutions. The CMIP5 models show similar correlations between RCP4.5 and RCP8.5. This means that both RCP4.5 and RCP8.5 show similar future changes in FOC: projected future changes in spatial distribution of FOC may be independent of emission scenarios. Regardless of emission scenarios, CMIP5 models tend to show significant negative correlations in the GL, NIO, SIO, SPO, and SAT, except for a few outliers. For all experiments, the correlations are generally stronger and more significant in the

NIO, SIO, SPO, and SAT than in the WNP, ENP, and NAT.

To reveal the quantitative contributions of the five factors in Eq. (4) to the projected future changes in basin-total FOCs, the contribution of each term was integrated over individual ocean basins, as shown in Fig. 5. For the MRI-AGCMs under the A1B scenario, the TC genesis effect (G_s) is the primary contributor to the projected total FOC change, indicating that projected changes in FOCs are proportional to the changes in FOGs, as also indicated by the results presented in Tables 2 and 3. The contribution of the nonlinear effect (N_s) is less than that of other terms, except in the SAT. The sum of signal terms (blue bars) is greater than that of bias terms (red bars), except in the SAT, indicating that the influence of model biases on basin-total FOC changes is small in the MRI-AGCMs. Patterns in the results of the CMIP5 models are similar to those observed in the MRI-AGCMs; however, the degree to which terms contribute to the basin-total FOC changes varies from model to model (e.g., models 4–7 show large contributions of the TC genesis effect in the GL, SIO, and SPO, whereas its contribution in other models is smaller). Moreover, the relative contribution of T_b or G_b (in terms of which is greater) varies according to the model and the ocean basin. The difference between the RCP4.5 and RCP8.5 scenarios is mostly small qualitatively, indicating that the contributions of each term to the total change are independent of emission scenarios. For the CMIP5 models showing increases in global FOCs under the RCP8.5 scenario (i.e., models 1, 2, and 11), each term contribution is different among the models. Model 2 shows the largest positive contribution from the signal of future change due to the TC genesis effect (G_s) in the three basins of GL, NIO, and WNP. Model 1 tends to show larger positive contributions from the model bias due to the TC track effect (T_b). In addition, the largest contribution in model 11 is G_s or signal of future change due to the TC track effect (T_s) in the three basins.

To show experimental variance in the degree of inheritance of model biases in the total change, Fig. 6 shows box plots of the values of the RBTC for the different ensembles and ocean basins. The overall sign of the median is consistent among the emission scenarios for each basin. For the GL, all experiments tend to show negative RBTC; the median of the RBTC is approximately -0.10 for all models, indicating that approximately 10% of the total future changes in FOCs are influenced by the model bias terms. The RBTCs are smaller in the SIO and SPO (<20%), which may be the result of marked future changes and, in part, to reduced model biases in these basins. Relatively large RBTCs are observed in the NAT and SAT, which may be the result of larger model biases in the FOCs in these basins. Positive RBTCs are observed in the NIO and SAT, indicating (from Fig. 2) that the models tend to overestimate projected future changes in these basins. In contrast, negative RBTCs are observed in the GL, WNP, ENP, and NAT, indicating that the models tend to underestimate projected future changes in these basins.

We examined how the bias terms are related to the performance of present-day simulations. Figure 7 reveals a relationship between the RBTC and the mean error (ME) of simulated present-day climatological FOCs relative to observations. The plots are eccentrically located in the first quadrant (ME > 0 and RBTC > 0) in the NIO, SIO, and SAT, indicating that, when a model overestimates the basin-total FOCs in the present-day simulation, the model also overestimates projected future changes in basin-total FOCs, regardless of the sign of the future changes and emission scenarios. The plots are also eccentrically located in the third quadrant (ME < 0 and RBTC < 0) in the GL, WNP, ENP, and NAT, indicating that, when a model underestimates the basin-total FOCs in the present-day simulation, the model also underestimates projected future changes in basin-total FOCs.

We examined how the bias terms affect the statistical significance of the projected future changes in FOCs. Figure 8 reveals relationships between the RBTCs and p values of the projected future changes. The numerous points have a V-shaped distribution and are located within the area of gray shading in the figure. This indicates that, when the bias terms are small relative to the total change, the total change tends to be statistically significant. In other words, to derive significant changes in FOCs in the future, model performance in the present-day simulation is critical.

d. Ensemble means using reliable models

The above analyses indicate that future changes projected by the models with smaller bias terms may be more reliable than those with larger bias terms on account of the smaller inheritance of biases by the projected future changes. On this basis, it may be reasonable to use the ensemble mean approach to analyze the data. With this approach, models with smaller bias terms are weighted more heavily in the generation of mean future projections.

At the bottoms of Tables 2 and 3, the ensemble means of changes in TC genesis frequencies and FOCs for each emission scenario are listed, according to different ensemble approaches [e.g., all models equally weighted (EQW), models with smaller bias terms (RBTC ≤ 0.5), and models with the five highest S_2 scores (S_2 Top5)]. Table 3 also provides information on the ratio of the bias terms to the total future change in FOC (i.e., RBTC);

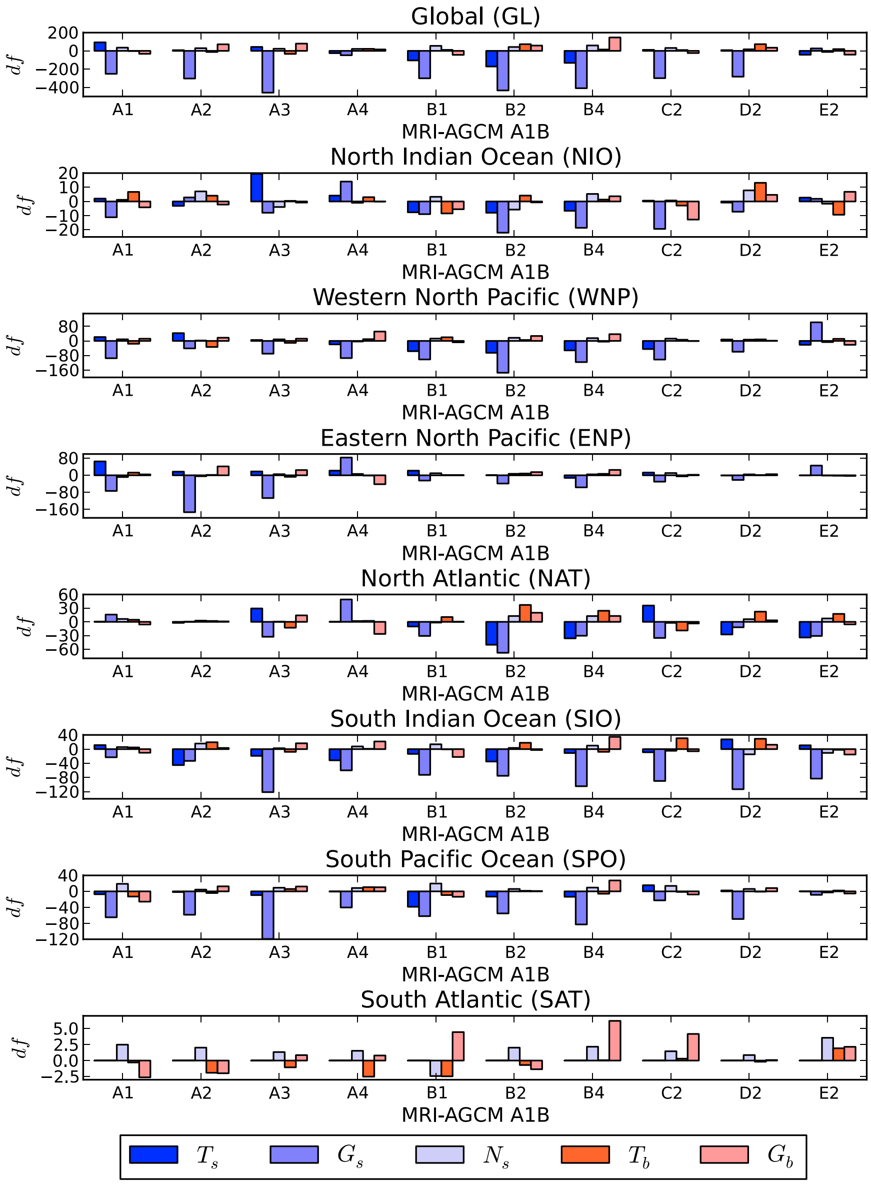

FIG. 5. The contribution of each term to the total change in FOC in each ocean basin (units: number per year). Factors that influence FOC changes are 1) the signals of future changes due to the TC track effect (T_s), TC genesis effect (G_s), and nonlinear effect (N_s) and 2) model biases due to the TC genesis effect (T_b) and the TC tracks effect (G_b). Blue bars represent terms for the signal of future changes, and red bars represent terms related to the biases (see the legend at the bottom of the figure).

the RBTC value may contribute useful information on the reliability of the projected future change. The ensemble mean result using EQW tends to show a higher level of significance when compared to individual experiments when most of the experiments show the same sign of the future change. When the ensemble mean is computed using RBTC ≤ 0.5 for the MRI-AGCM A1B scenario, the mean value is not so different from either EQW or S_2 Top5, implying that weighing has a lower impact on results. This is consistent with findings of previous studies that unequal weights do not show significant improvement over equal weights (DelSole et al. 2013), although equal weights may be the safer and more transparent way to combine models (Weigel and Knutti 2010). However, the future change using RBTC ≤ 0.5 becomes less significant ($p = 0.24$) in the SAT, where models systematically overestimate FOCs, leading to more reliable future projections in terms of statistical

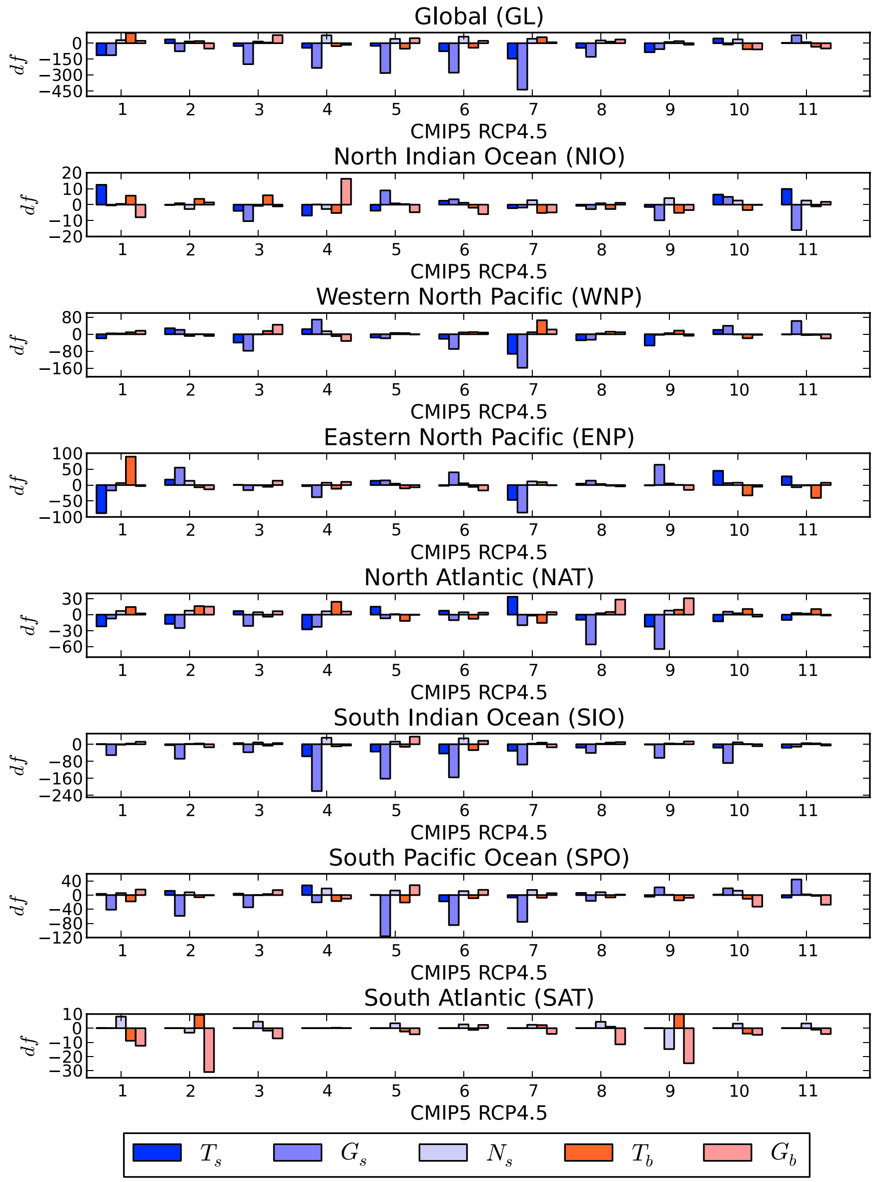

FIG. 5. (*Continued*)

significance. The degree of inheritance of model biases in the total change in FOCs is also smaller for RBTC ≤ 0.5 compared with other ensembles. The ensemble mean with RBTC ≤ 0.5 shows 7, 7, and 8 ocean basins showing RBTC < 0.25 for MRI-AGCM A1B, CMIP5 RCP4.5, and CMIP5 RCP8.5, respectively. The ensemble mean with EQW (S_2 Top5) shows 6, 6, and 5 (7, 4, and 4) basins showing RBTC < 0.25 for each scenario. This indicates greater confidence in the quantitative discussion on future changes using ensemble approach with RBTC ≤ 0.5 compared with other ensemble approaches.

Overall, significant decreases in the basin-total FOCs and TC genesis frequencies are limited to the GL, WNP, SIO, and SPO for the MRI-AGCM A1B scenario. The CMIP5 RCP4.5 scenario obtains mostly similar results except that NAT tends to show statistically more significant (p = 0.0–0.09) changes in both ensemble approaches for TC genesis number. The marked difference between the ensemble approaches for CMIP5 RCP4.5 is the degree of changes in GL, SPO, and NAT: RBTC ≤ 0.5 and S_2 Top5 show larger negative changes than EQW in the GL, and RBTC ≤ 0.5 shows larger negative changes than EQW and S_2 Top5 in the SPO. This is mainly because selected models where RBTC ≤ 0.5 (e.g., models 4, 5, 6, 7, and 9 for GL and models 1, 2, 5, 6, and 7 for SPO) show marked projected decreases in both

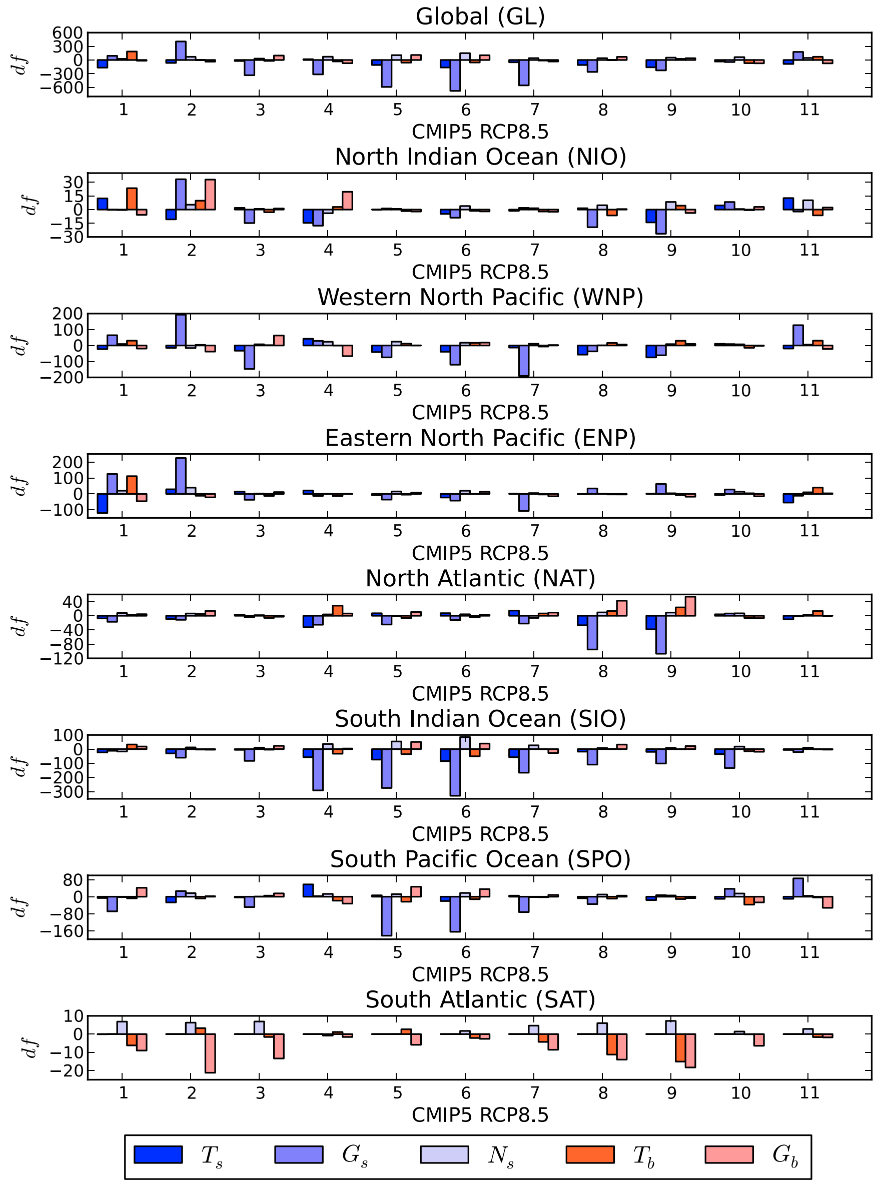

FIG. 5. (*Continued*)

TC genesis frequency and FOCs (Tables 2, 3). Similar differences between the ensemble approaches are also seen in CMIP5 RCP8.5. Moreover, the difference is also clear in the NIO, where both EQW and S_2 Top5 show projected future increases, whereas RBTC $\leq$ 0.5 shows significant (p = 0.0–0.016) decreases. This is mainly because the ensemble with RBTC $\leq$ 0.5 does not include model 2, which shows marked increases in TC genesis frequency and FOCs in the NIO.

Figure 9 shows the spatial distribution of the projected future changes in FOCs using the ensemble mean approaches (note that the models with RBTC $\leq$ 0.5 and S_2 Top5 used to calculate the ensemble mean are different for each ocean basin); the regions of enhanced reliability in the projected future changes are shaded white (i.e., statistically significant changes with reduced inheritance of model biases in the future changes). The difference between the ensemble approaches is small qualitatively; however, the ensemble mean using RBTC $\leq$ 0.5 shows larger decreases in FOCs in the SPO compared with that using EQW and S_2 Top5 as discussed previously.

The results from Fig. 9 also show mostly robust spatial patterns regardless of the emission scenarios. The projected reductions in FOCs are significant in the WNP (p = 0.007–0.05), SIO (p = 0.003–0.02), and SPO (p = 0.006–0.04), which is consistent with previous studies

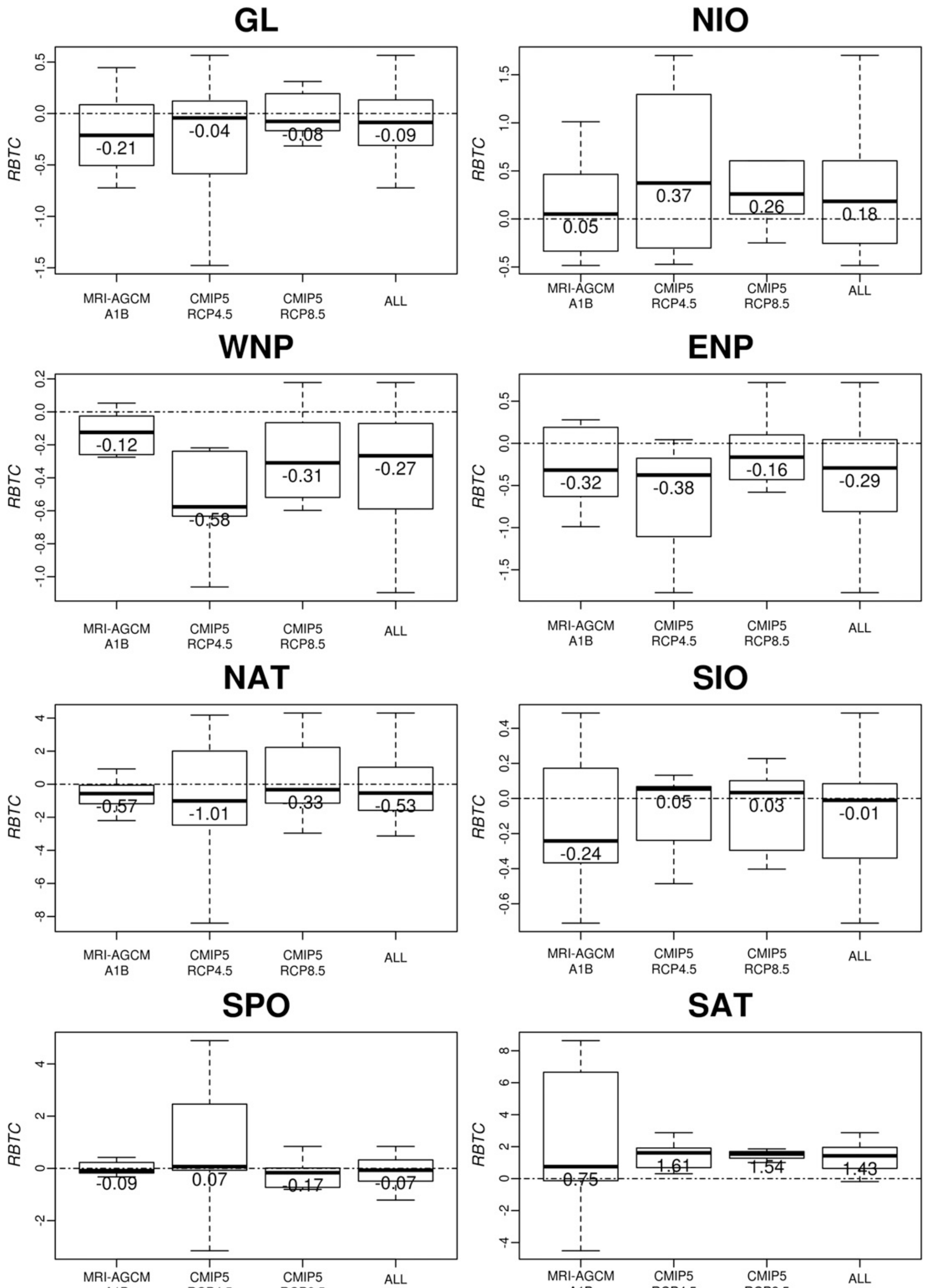

FIG. 6. Box plots of the ratio of the bias terms to the projected future change for each basin. Each panel shows ensemble approaches using the MRI-AGCM A1B, CMIP5 RCP4.5, and CMIP5 RCP8.5, and the combined data of both models (all). The boxes represent the lower and upper quartiles, the horizontal lines show the median value, and the dashed bars show the lowest datum still within the 1.5 interquartile range (IQR) of the lower quartile and the highest datum still within the 1.5 IQR of the upper quartile. Outliers are omitted in the plots, as data points do not appear to be represented in the plots.

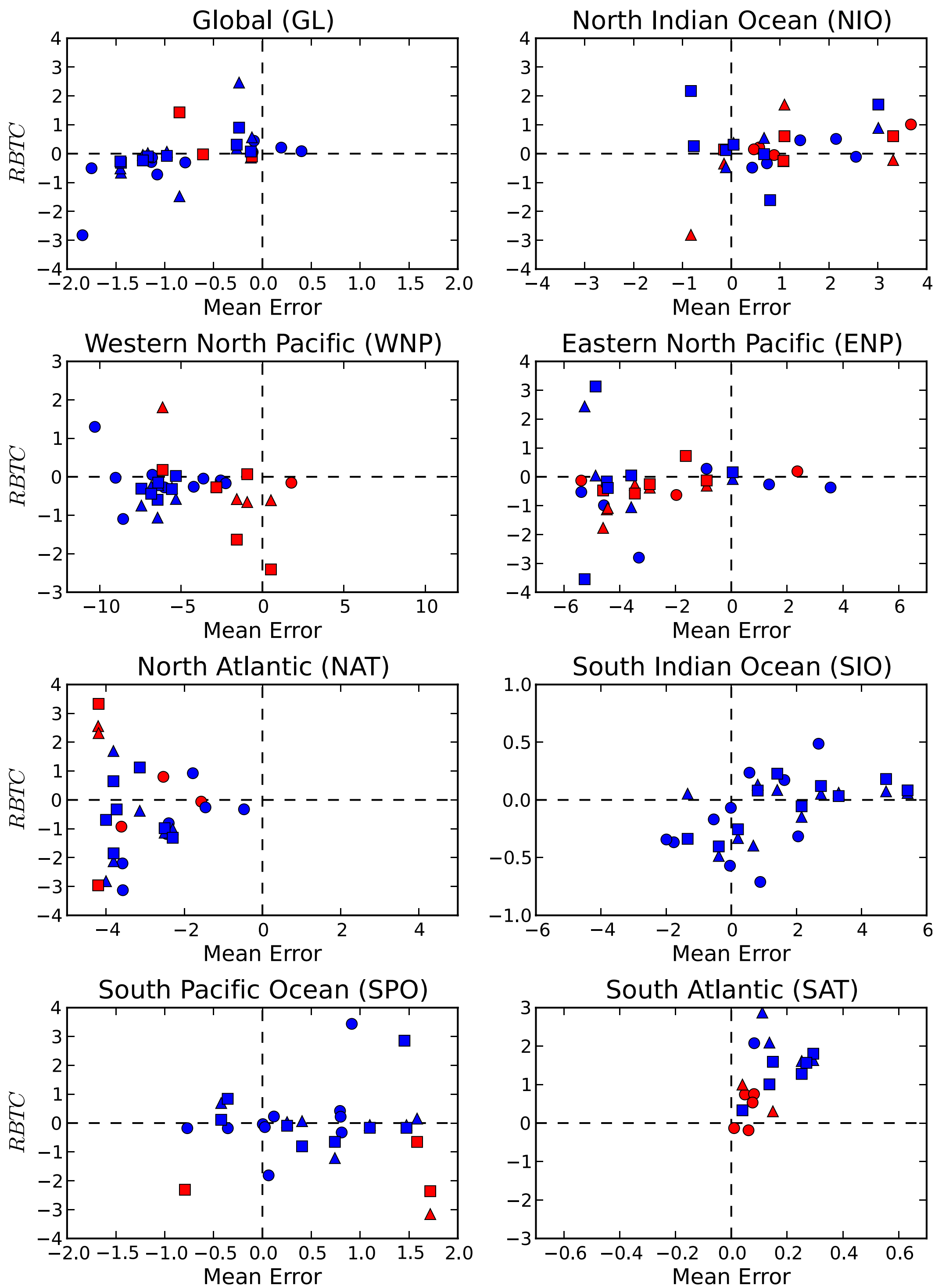

FIG. 7. Scatter diagrams showing the relationships between the mean error in the FOC in the present-day simulations and the ratio of the bias term to the basin-total projected future change in each basin. Red (blue) dots indicate that the model projects a decrease (increase) in the basin-total FOC. Symbols indicate experiments by MRI-AGCM A1B (circles), CMIP5 RCP4.5 (triangles), and CMIP5 RCP8.5 (squares).

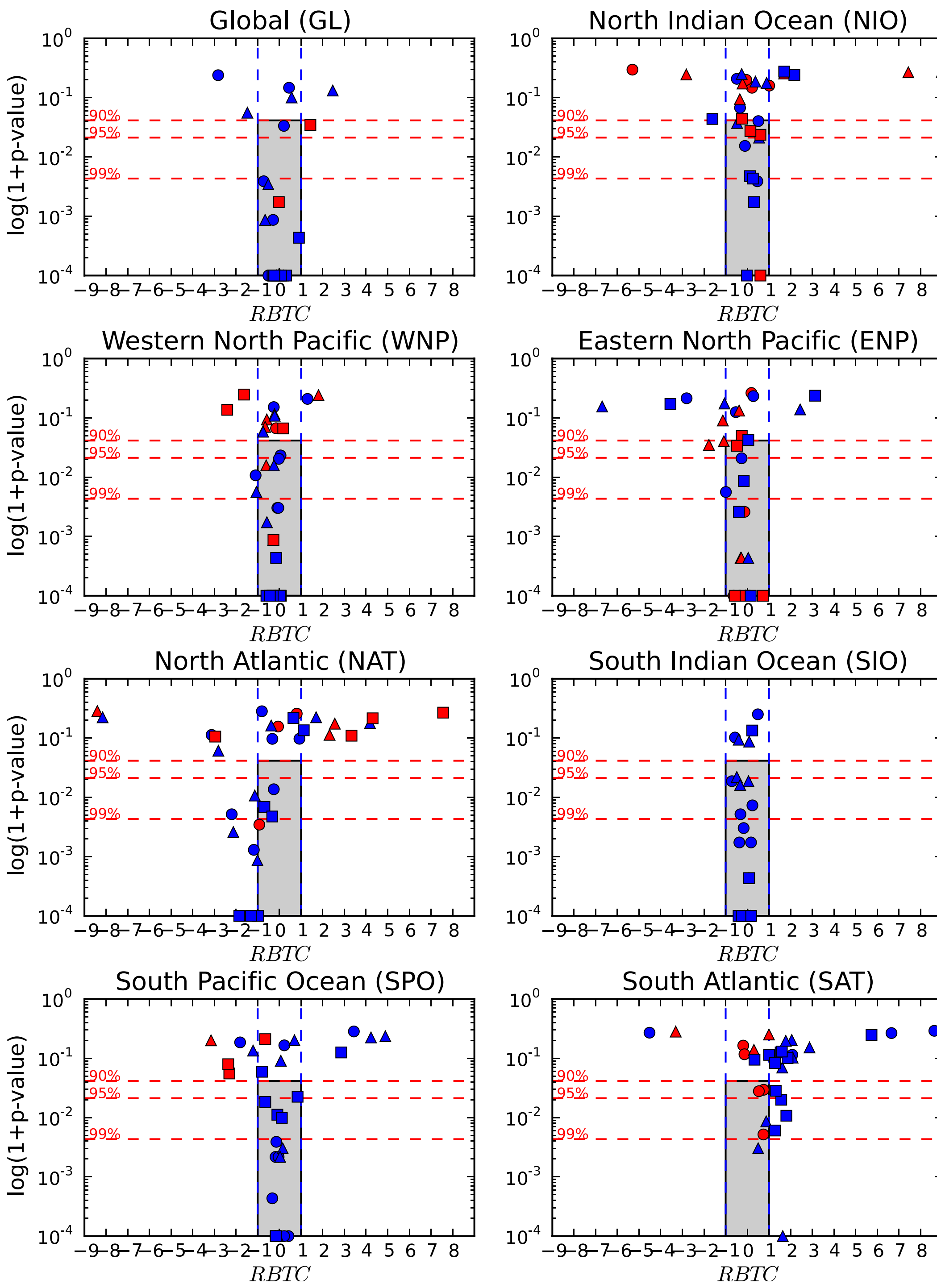

FIG. 8. Relationship between the ratio of the bias term to the basin-total future change and the p value [log(1 + p value)] for the projected future change in the basin-total FOC. Red dashed lines indicate significance levels of 90%, 95%, and 99%. The gray shading indicates that the projected future change is statistically significant and that the changes contain fewer model biases ($|\mathrm{RBTC}| < 1.0$). Note that a few points plotted outside of the region (because of the large RBTC) are not shown in the figure.

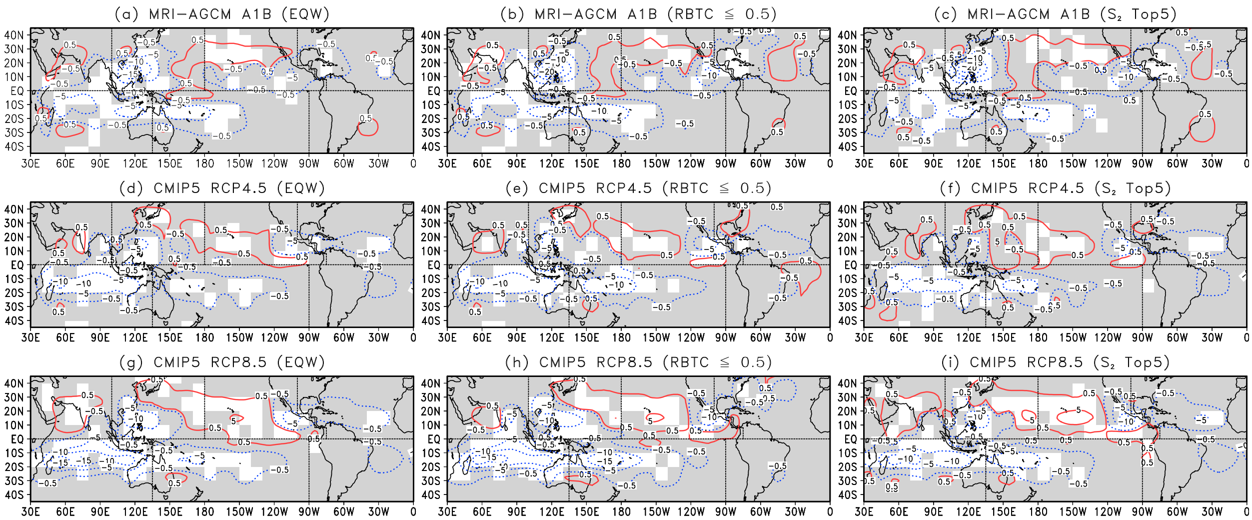

FIG. 9. Ensemble means of projected future changes in the FOC by MRI-AGCMs under A1B scenario, using (a) all models equally weighted, (b) the models with RBTC ≤ 0.5 in each basin, and (c) the top five S_2 models in each basin. (d)–(f) As in (a)–(c), but for CMIP5 RCP4.5. (g)–(i) As in (a)–(c), but for CMIP5 RCP8.5. For the ensembles, except for EQW, the composite was constructed from the mean values for each basin but the means were calculated using different models in each basin. The white shading indicates regions with a statistically significant change (at the 90% confidence level or above, as determined by the bootstrap method) and gives an indication of the lower bias term as compared with the total future changes (i.e., RBTC ≤ 0.5). Unit: number per year.

(Knutson et al. 2010; Murakami et al. 2012a). An eastward shift in the maximum density of FOCs in the WNP, which has been noted previously (Yokoi and Takayabu 2009; Murakami et al. 2011; Yokoi et al. 2012; Mori et al. 2013), can be recognized for all emission scenarios. The FOC changes near Japan, however, are inconsistent between the MRI-AGCM and CMIP5 models. The ensemble mean results also robustly show a projected westward shift in the maximum density of FOCs in the NIO (i.e., an increase in FOCs in the Arabian Sea and a decrease in FOCs in the Bay of Bengal), a trend that was also reported by Murakami et al. (2013a). An eastward shift in the maximum FOCs in the NAT, as discussed in previous studies (Murakami and Wang 2010; Colbert et al. 2013), is only apparent in the MRI-AGCM A1B scenario but with less significance (p = 0.3), although all of the emission scenarios robustly show a projected decrease in FOCs in the Caribbean Sea. Recently, Murakami et al. (2013b) reported a projected increase in FOCs over the central subtropical Pacific (in the vicinity of the Hawaiian Islands), a trend that is also predicted in all experiments regardless of emission scenarios.

In summary, the following projected future changes in FOCs appear to be the most significant and reliable on the basis of our analysis: decreases in FOCs in the Bay of Bengal, WNP, eastern portion of the ENP, Caribbean Sea, SIO, and SPO and increases in FOCs in the Arabian Sea and subtropical central Pacific.

4. Summary

In this study, the inheritance of model biases by the results of projected future changes in FOCs was investigated using a new empirical statistical analysis. We based our results on 25-yr present-day simulations and future projections for the last quarter of twenty-first century from 10 MRI-AGCMs under the A1B scenario and 11 CMIP5 models under the RCP4.5 and RCP8.5 scenarios.

Overall, the models project statistically significant decreases in basin-total FOCs and TC genesis frequencies globally (by 15%–29% for A1B; by 6%–23% for RCP4.5; and by 13%–40% for RCP8.5) and the Southern Hemisphere ocean basins showed a marked decrease compared with the Northern Hemisphere ocean basins, a result that is consistent with previous studies (e.g., Knutson et al. 2010). Most of the MRI-AGCMs under the A1B scenario project significant reductions in TC genesis frequencies and basin-total FOCs in the WNP and ENP; however, the degree and extent of the changes projected by the models vary widely. On the other hand, CMIP5 modes under RCP4.5 and RCP8.5 show diverse results in the WNP and ENP: even the mean change sign is different among models, indicating that projected future changes in FOCs at basin scale are model dependent and remain uncertain.

Spatial correlation coefficients between model biases in FOCs and projected future changes reveal that the sign of the correlation varies according to the model version: namely, model physics for MRI-AGCMs under the A1B scenario, which indicates a large impact by model physics on results. The CMIP5 models robustly show negative correlations in the GL, NIO, SIO, SPO, and SAT. The correlations are similar between RCP4.5 and RCP8.5 scenarios, indicating that spatial patterns of projected future changes in FOCs are independent on emission scenarios.

A newly developed empirical statistical analysis was used to investigate the quantitative contribution of five factors to the projected future changes in basin-total FOCs. Most of the experiments show larger contributions from the term related to signals of future changes by TC genesis frequency than from other terms, indicating that projected changes in TC genesis frequency is the primary contributor to the projected changes in basin-total FOCs. The analysis of the ratio of the summed magnitudes of the bias terms to the magnitudes of the total future change in FOCs (RBTC) reveals that approximately 10% of the total future change in global FOC is influenced by model biases in the present-day simulations. The inheritance of model biases is less in the SIO and SPO (<20%), which suggests that projected future changes in FOCs in these basins are more reliable. The analysis also indicates that projected future changes in FOCs tend to be overestimated by the models in the NIO (by approximately +18%) and SAT (+143%), whereas they tend to be underestimated in the WNP (−27%), ENP (−29%), and NAT (−53%).

We investigated the relationship between the RBTC and the mean error of simulated present-day climatological FOCs. The results indicate that, when a model overestimates (underestimates) FOCs in the present-day simulations, the model also overestimates (underestimates) future changes in FOCs. We also investigated the relationship between the RBTC and the statistical significance of the projected future changes in basin-total FOCs. Our results imply that minimizing model biases in present-day simulations is critical to deriving significant signals of future changes.

Finally, an ensemble mean analysis was conducted to obtain more reliable projections, using 1) an equally weighted ensemble mean, 2) models with smaller bias terms, and 3) models with the five highest S_2 scores. Overall, on the basis of the ensemble mean results, the following projected future changes appear to be most significant and reliable: decreases in the FOCs in the Bay of Bengal, WNP, eastern portion of the ENP, Caribbean Sea, SIO, and SPO and increases in FOCs in the Arabian Sea and subtropical central Pacific.

Our study did not consider biases in the future projections resulting from an absence of observed information in the future. An investigation of these biases might be important in order to determine whether a model preserves the same (or similar) biases observed at present in the different climate regimes or under different rates of anthropogenic/natural forcings. However, observations of global TC tracks are limited prior to the commencement of satellite-based observations in the 1970s. This is a topic to be addressed in future studies.

Our study also did not consider differences in TC-detection schemes, which may introduce some uncertainties into projected future changes. For example, Camargo (2013) shows relative increases in projected global TC genesis frequency for a few CMIP5 models (MPI-ESM-LR and MRI-CGCM3) for both the RCP4.5 and RCP8.5 scenarios based on the use of the detection algorithm of Camargo and Zebiak (2002), although these changes are not statistically significant. Our detection algorithms, however, do not show such increases for these models. Tory et al. (2013) also analyzed TC genesis frequencies for the CMIP5 models under the RCP8.5 scenario using a unique TC-detection method incorporating large-scale TC formation conditions. They reported that eight reliable CMIP5 models commonly project decreases in global TC frequency. However, as pointed out by Tory et al. (2013), a large number of higher latitude TCs (e.g., subtropical systems) were detected in the late twenty-first century under the RCP8.5 scenario without any inclusions of adjustments for their detection method. If these subtropical systems were included, the results might mislead researchers to conclude an increase in global TC frequency.

Apart from the differences in TC-detection methods, Emanuel (2013) recently reported, using a statistical–dynamical downscaling technique, that downscaling CMIP5 models under the RCP8.5 scenario robustly projects increases in global TC frequency, whereas downscaling CMIP3 models under the A1B scenario robustly projects decreases in global TC frequency. These uncertainties in differences in TC-detection methods, emission scenarios, and model framework should be further clarified to obtain more reliable projections of future changes in TC activity.

Acknowledgments. This work was conducted under the framework of the ''Projection of the Change in Future Weather Extremes Using Super-High-Resolution Atmospheric Models'' supported by the KAKUSHIN and SOUSEI programs of the Ministry of Education, Culture, Sports, Science, and Technology (MEXT) of Japan and sponsored by ONR Grant N000141210450. Calculations were performed on the Earth Simulator. H.M. was supported by the ''Research on Prediction of Climate and Environmental Change to Contribute to

Mitigation Plan Decision against Climate Change'' of the MRI of Japan. H.M. would like to thank the U.S. CLIVAR Hurricane Workshop for supporting his attendance at a workshop. H.M. thanks Ms. May Izumi for her editorial service. P.-C. H. was partly supported by the NSFC (Grant 41375100) and Research Project of Chinese Ministry of Education (213014A).

REFERENCES

Arakawa, A., and W. H. Schubert, 1974: Interaction of cumulus cloud ensemble with the large-scale environment. Part I. *J. Atmos. Sci.,* **31,** 674–701.

Bender, M. A., T. R. Knutson, R. E. Tuleya, J. J. Sirutis, G. A. Vecchi, S. T. Garner, and I. M. Held, 2010: Modeled impact of anthropogenic warming on the frequency of intense Atlantic hurricanes. *Science,* **327,** 454–458.

Bengtsson, L., M. Botzet, and M. Esch, 1996: Will greenhouse gas-induced warming over the next 50 years lead to higher frequency and greater intensity of hurricanes? *Tellus,* **48A,** 57–73.

Camargo, S. J., 2013: Global and regional aspects of tropical cyclone activity in the CMIP5 models. *J. Climate,* **26,** 9880–9902.

——, and S. E. Zebiak, 2002: Improving the detection and tracking of tropical cyclones in atmospheric general circulation models. *Wea. Forecasting,* **17,** 1152–1162.

Casanova, S., and B. Ahrens, 2009: On the weighting of multimodel ensembles in seasonal and short-range weather forecasting. *Mon. Wea. Rev.,* **137,** 3811–3822.

Chen, W., Z. Jiang, and L. Li, 2011: Probabilistic projections of climate change over China under the SRES A1B scenario using 28 AOGCMs. *J. Climate,* **24,** 4741–4756.

Colbert, A. J., B. J. Soden, G. A. Vecchi, and B. P. Kirtman, 2013: The impact of anthropogenic climate change on North Atlantic tropical cyclone tracks. *J. Climate,* **26,** 4088–4095.

DelSole, T., X. Yang, and M. K. Tippet, 2013: Is unequal weighting significantly better than equal weighting for multi-model forecasting? *Quart. J. Roy. Meteor. Soc.,* **139,** 176–183.

Emanuel, K. A., 2013: Downscaling CMIP5 climate models show increased tropical cyclone activity over the 21st century. *Proc. Natl. Acad. Sci. USA,* **110,** 12 219–12 224, doi:10.1073/pnas.1301293110.

——, R. Sundararajan, and J. Williams, 2008: Hurricanes and global warming: Results from downscaling IPCC AR4 simulations. *Bull. Amer. Meteor. Soc.,* **89,** 347–367.

Giorgi, F., and L. O. Mearns, 2003: Probability of regional climate change based on the reliability ensemble averaging (REA) method. *Geophys. Res. Lett.,* **30,** 1629, doi:10.1029/2003GL017130.

Kain, J. S., and J. M. Fritsch, 1990: A one-dimensional entraining/detraining plume model and its application in convective parameterization. *J. Atmos. Sci.,* **47,** 2784–2802.

Knutson, T. R., and Coauthors, 2010: Tropical cyclones and climate change. *Nat. Geosci.,* **3,** 157–163.

——, and Coauthors, 2013: Dynamical downscaling projections of twenty-first-century Atlantic hurricane activity: CMIP3 and CMIP5 model-based scenarios. *J. Climate,* **26,** 6591–6617.

Li, T., M. Kwon, M. Zhao, J.-S. Kug, J.-J. Luo, and W. Yu, 2010: Global warming shifts Pacific tropical cyclone location. *Geophys. Res. Lett.,* **37,** L21804, doi:10.1029/2010GL045124.

Meehl, G. A., C. Covey, K. E. Taylor, T. Delworth, R. J. Stouffer, M. Latif, B. McAvaney, and J. F. B. Mitchell, 2007: The WCRP CMIP3 multimodel dataset: A new era in climate change research. *Bull. Amer. Meteor. Soc.,* **88,** 1383–1394.

Mizuta, R., and Coauthors, 2006: 20-km-mesh global climate simulations using JMA-GSM model: Mean climate states. *J. Meteor. Soc. Japan,* **84,** 165–185.

——, Y. Adachi, S. Yukimoto, and S. Kusunoki, 2008: Estimation of the future distribution of sea surface temperature and sea ice using the CMIP3 multi-model ensemble mean. Meteorological Research Institute Tech. Rep. 56, 36 pp. [Available online at http://www.mri-jma.go.jp/Publish/Technical/DATA/VOL_56/tec_rep_mri_56.pdf.]

——, and Coauthors, 2012: Climate simulations using MRI-AGCM3.2 with 20-km grid. *J. Meteor. Soc. Japan,* **90A,** 233–258.

Mori, M., and Coauthors, 2013: Hindcast prediction and near-future projection of tropical cyclone activity over the western North Pacific using CMIP5 near-term experiments with MIROC. *J. Meteor. Soc. Japan,* **91,** 431–452.

Murakami, H., and M. Sugi, 2010: Effect of model resolution on tropical cyclone climate projections. *SOLA,* **6,** 73–76.

——, and B. Wang, 2010: Future change of North Atlantic tropical cyclone tracks: Projection by a 20-km-mesh global atmospheric model. *J. Climate,* **23,** 2699–2721.

——, ——, and A. Kitoh, 2011: Future change of western North Pacific typhoons: Projections by a 20-km-mesh global atmospheric model. *J. Climate,* **24,** 1154–1169.

——, R. Mizuta, and E. Shindo, 2012a: Future changes in tropical cyclone activity projected by multi-physics and multi-SST ensemble experiments using the 60-km-mesh MRI-AGCM. *Climate Dyn.,* **39,** 2569–2584, doi:10.1007/s00382-011-1223-x.

——, and Coauthors, 2012b: Future changes in tropical cyclone activity projected by the new high-resolution MRI-AGCM. *J. Climate,* **25,** 3237–3260.

——, M. Sugi, and A. Kitoh, 2013a: Future changes in tropical cyclone activity in the north Indian Ocean by high-resolution MRI-AGCMs. *Climate Dyn.,* **40,** 1949–1968.

——, B. Wang, T. Li, and A. Kitoh, 2013b: Projected increase in tropical cyclones near Hawaii. *Nat. Climate Change,* **3,** 749–754.

Oouchi, K., J. Yoshimura, H. Yoshimura, R. Mizuta, S. Kusunoki, and A. Noda, 2006: Tropical cyclone climatology in a global-warming climate as simulated in a 20km-mesh global atmospheric model: Frequency and wind intensity analysis. *J. Meteor. Soc. Japan,* **84,** 259–276.

Perkins, S. E., and A. J. Pitman, 2009: Do weak AR4 models bias projections of future climate changes over Australia? *Climatic Change,* **93,** 527–558.

Raftery, A. E., T. Gneiting, F. Balabdaous, and M. Polakowski, 2005: Using Bayesian model averaging to calibrate forecast ensembles. *Mon. Wea. Rev.,* **133,** 1155–1172.

Räisänen, J., L. Ruokolainen, and J. Ylhäisi, 2010: Weighting of model results for improving best estimates of climate change. *Climate Dyn.,* **35,** 407–422.

Randall, D., and D.-M. Pan, 1993: Implementation of the Arakawa-Schubert cumulus parameterization with a prognostic closure. *The Representation of Cumulus Convection in Numerical Models, Meteor. Monogr.,* No. 46, Amer. Meteor. Soc., 137–144.

Rayner, N. A., D. E. Parker, E. B. Horton, C. K. Folland, L. V. Alexander, and D. P. Rowell, 2003: Global analysis of sea surface temperature, sea ice, and night marine air temperature since the late nineteenth century. *J. Geophys. Res.,* **108,** 4407, doi:10.1029/2002JD002670.

Santer, B. D., and Coauthors, 2009: Incorporating model quality information in climate change detection and attribution studies. *Proc. Natl. Acad. Sci. USA,* **106,** 14 778–14 783.

Schmittner, A., M. Latif, and B. Schneider, 2005: Model projections of the North Atlantic thermohaline circulation for the 21st century assessed by observations. *Geophys. Res. Lett.,* **32,** L23710, doi:10.1029/2005GL024368.

Solomon, S., D. Qin, M. Manning, Z. Chen, M. Marquis, K. Averyt, M. Tignor, and H. L. Miller Jr., Eds., 2007: *Climate Change 2007: The Physical Science Basis.* Cambridge University Press, 996 pp.

Sugi, M., H. Murakami, and J. Yoshimura, 2009: A reduction in global tropical cyclone frequency due to global warming. *SOLA,* **5,** 164–167.

Taylor, K. E., 2001: Summarizing multiple aspects of model performance in a single diagram. *J. Geophys. Res.,* **106** (D7), 7183–7192.

——, R. J. Stouffer, and G. A. Meehl, 2012: An overview of CMIP5 and the experiment design. *Bull. Amer. Meteor. Soc.,* **93,** 485–498.

Tippet, M. K., 2006: Filtering of GCM simulated Sahel precipitation. *Geophys. Res. Lett.,* **33,** L01804, doi:10.1029/2005GL024923.

——, L. Goddard, and A. G. Barnston, 2005: Statistical–dynamical seasonal forecasts of central-southwest Asian winter precipitation. *J. Climate,* **18,** 1831–1843.

Tory, K., S. Chand, J. McBride, H. Ye, and R. Dare, 2013: Projected changes in late-twenty-first-century tropical cyclone frequency in 13 coupled climate models from the Coupled Model Intercomparison Project Phase 5. *J. Climate,* **26,** 9946–9959.

Unisys, cited 2013: Unisys weather hurricane tropical data. [Available online at http://weather.unisys.com/hurricane/].

Walsh, K., S. Lavender, E. Scoccimarro, and H. Murakami, 2013: Resolution dependence of tropical cyclone formation in CMIP3 and finer resolution models. *Climate Dyn.,* **40,** 585–599.

Weigel, A. P., and R. Knutti, 2010: Risks of model weighing in multimodel climate projections. *J. Climate,* **23,** 4175–4191.

Whetton, P., I. Macadam, J. Bathols, and J. O'Grady, 2007: Assessment of the use of current climate patterns to evaluate regional enhanced greenhouse response patterns of climate models. *Geophys. Res. Lett.,* **34,** L14701, doi:10.1029/2007GL030025.

Yokoi, S., and Y. N. Takayabu, 2009: Multi-model projection of global warming impact on tropical cyclone genesis frequency over the western North Pacific. *J. Meteor. Soc. Japan,* **87,** 525–538.

——, and ——, 2013: Attribution of decadal variability in tropical cyclone passage frequency over the western North Pacific: A new approach emphasizing the genesis location of cyclones. *J. Climate,* **26,** 973–987.

——, C. Takahashi, K. Yasunaga, and R. Shirooka, 2012: Multi-model projection of tropical cyclone genesis frequency over the western North Pacific: CMIP5 results. *SOLA,* **8,** 137–140.

Yukimoto, S., and Coauthors, 2011: Meteorological Research Institute-Earth System Model v1 (MRI-ESM1): Model description. Meteorological Research Institute Tech. Rep. 64, 96 pp. [available at http://www.mri-jma.go.jp/Publish/Technical/DATA/VOL_64/tec_rep_mri_64.pdf.]

Zhao, M., and I. M. Held, 2012: TC-permitting GCM simulations of hurricane frequency response to sea surface temperature anomalies projected for the late-twenty-first century. *J. Climate,* **25,** 2995–3009.

——, ——, S.-J. Lin, and G. A. Vecchi, 2009: Simulations of global hurricane climatology, interannual variability, and response to global warming using a 50-km resolution GCM. *J. Climate,* **22,** 333–363.